

Chatter Stability of Machining Operations

Dedicated to S.A. Tobias and J. Tlusty

Yusuf Altintas, (lead)

Professor, Fellow ASME

The University of British Columbia

Department of Mechanical Engineering

Manufacturing Automation Laboratory (MAL)

2054-6250 Applied Science Lane

Vancouver BC V6T 1Z4 Canada

altintas@mech.ubc.ca

Gabor Stepan,

Professor of Applied Mechanics, Budapest University of Technology and Economics

stepan@mm.bme.hu

Erhan Budak,

Professor, Faculty of Engineering and Natural Sciences, Sabanci University, Turkey

ebudak@sabanciuniv.edu

Tony Schmitz,

Professor, Fellow ASME

University of Tennessee, Knoxville

Joint Faculty, Oak Ridge National Laboratory

tony.schmitz@utk.edu

Zekai Murat Kilic,

Lecturer, University of Manchester,

zekaimurat.kilic@manchester.ac.uk

Abstract

This paper reviews the dynamics of machining and chatter stability research since the first stability laws were introduced by Tlusty and Tobias in the 1950s. The paper aims to introduce the fundamentals of dynamic machining and chatter stability, as well as the state of the art and research challenges, to readers who are new to the area. First, the unified dynamic models of mode coupling and regenerative chatter are introduced. The chatter stability laws in both the frequency and time domains are presented. The dynamic models of intermittent cutting, such as milling, are presented and their stability solutions are derived by considering the time-periodic behavior. The complexities contributed by highly intermittent cutting, which leads to additional stability pockets, and the contribution of the tool's flank face to process damping are explained. The stability of parallel machining operations is explained. The design of variable pitch and serrated cutting tools to suppress chatter is presented. The paper concludes with current challenges in chatter stability of

machining which remains to be the main obstacle in increasing the productivity and quality of manufactured parts.

1. Introduction

Chatter continues to be the main limitation in increasing material removal rates, productivity, surface quality, and dimensional accuracy of machined parts. F. W. Taylor, who was considered to be the initiator of manufacturing engineering, declared that chatter was the “most obscure and delicate of all problems facing the machinist” in his 1906 ASME article [1]. The early investigations on chatter mechanisms were conducted by Arnold [2], who classified machining vibrations as forced and self-induced types. He conducted several turning experiments at varying speeds and feeds and reported the influence of cutting conditions and tool wear on the shape of the vibration waves and stability. Doi and Kato presented the effect of time lag in the thrust force relative to the chip thickness variation as the source of chatter instability in turning [3]. The first scientific stability laws were independently presented at almost at the same time by Tobias *et al.* [4] and Tlusty *et al.* [5] in the 1950s. Tlusty presented an absolute stability law that predicted the critical depth of cut proportional to the machine’s dynamic stiffness and inversely proportional to the material’s cutting force coefficient in orthogonal cutting regardless of the spindle speed. Tobias presented a similar stability law, but included the effect of spindle speed, i.e., the regenerative time delay, which led to the stability pockets or “lobes” in orthogonal cutting. The dynamics of cutting and chatter stability models were reviewed by Tlusty [6, 7] and Altintas and Weck [8]. General literature reviews on the sources of nonlinearities in the dynamics of cutting [9] and chatter [10] were also presented. Altintas *et al.* presented the frequency and time domain chatter stability prediction laws [11].

The chatter theories have been applied to the analysis of machine tools to improve their dynamic stiffness through design modifications or by adding passive and active dampers. Machine tools are dynamically tested; the critical mode shapes which affect their chatter stability are identified and modified to strengthen their stiffness by machine tool designers. Merritt converted the stability equations of Tlusty and Tobias into a closed-loop system with unity and delayed feedback to consider regeneration and solved the stability using the Nyquist criterion [12]. Tlusty showed that the productivity gain is proportional to the dynamic stiffness improvements at the tool-workpiece contact zone in the direction of chip generation [13]. The dynamics of various metal cutting and grinding operations have been modeled by several researchers and their stability was solved by applying the one-dimensional, frequency domain stability laws of Tlusty and Tobias. Tlusty pioneered the development of high-speed milling machines by stating that the product of spindle speed and the number of teeth on the cutter (i.e., the tooth passing frequency) should be matched with the first bending mode of the spindle to operate the machine at the highest speed (first, or rightmost) lobe which leads to highest material removal rate [7]. High speed-high power spindles were developed to remove more than 95% of the material from aluminum slabs to produce monolithic, lightweight parts for the aerospace industry [14, 15]. As the application domains have grown, the limitation of Tobias’s and Tlusty’s one-dimensional stability theories have also been investigated. It was observed that as the spindle speed is reduced relative to the natural frequency of the machine, the stability of the process increases due to process damping. Tobias attributed this process damping effect to the penetration of the cutting edge into the wavy cut surface [16] which is still studied at the present. Process damping significantly depends on the ratio of the cutting speed to the chatter frequency caused by the dominant mode. In the presence of low-frequency

modes for multi-mode systems, the process damping effect may not be observed at low speeds as would be expected. Munoa *et al.* [17] noted that if the tooth passing frequency is low relative to the natural frequency of the mode, the process damping may stabilize the cutting process. On the other hand, if the tooth passing frequency is several times higher than the natural frequency, the mode can hardly create chatter problems. Tunc *et al.* [18] showed that when the high-frequency mode is suppressed by the process damping effect, the chatter mode shifts to the low-frequency mode even if the low-frequency mode is more rigid. This is critically important when machining thin-wall parts.

Sridhar [19] showed that milling operations have coupled dynamics in two directions with periodic coefficients; therefore, the stability of such multi-point machining applications cannot be solved by the one-dimensional chatter theories of Tlusty and Tobias. Minis and Yanushevsky [20, 21] applied Floquet theory to solve the stability of two dimensional, periodic milling operations in the frequency domain. Budak and Altintas determined the stability limit by considering the harmonics of tooth passing frequencies in the eigenvalues [22, 23], as well as a direct solution of stability analytically by considering the averages of directional factors [24] in the frequency domain. The research group of Stepan presented a semi-discrete time-domain stability solution of a single [25] and two-directional milling operations [26]. The research in chatter stability continues due to its complexity and application to the design of machine tools and cutting tools, as well as their chatter-free and productive use in machining operations.

The aim of this paper is not a general review of the chatter literature, but rather the presentation of mathematical modeling of the dynamic cutting process and its stability solution in the frequency and time domains; see Sections 2 and 3. The mechanism behind the appearance of stability islands for highly intermittent cutting operations at high spindle speeds is explained in Sections 2.3 and 3.3. The design of special-purpose cutters to suppress chatter is presented with the aid of stability models in Section 4, and the complexities of parallel machining dynamics are discussed in Section 5. The paper is intended to provide strong foundations in dynamic cutting and chatter stability while explaining the current research challenges including improved accuracy (Section 6). The paper is concluded in Section 7 by pointing out the future challenges in chatter research. The paper is dedicated to the two pioneering scientists, the late Professors Tobias and Tlusty, who contributed immensely to chatter stability literature that led to the present high-speed machine tool and high-performance machining technologies.

2. Chatter Stability of Orthogonal Cutting

A general diagram of a single point cutting system, where the tool edge is orthogonal to the cutting speed v_c and the chip thickness varies normal to the velocity in the direction r , is shown in Figure 1a. The system is assumed to have multiple flexibilities in directions x_i with an inclination angle of θ_i from the velocity direction. The tangential (F_t) and thrust (F_r) forces act in the directions of cutting velocity (v_c) and its normal (r), respectively. The resultant cutting force ($F_c = \sqrt{F_t^2 + F_r^2}$) has an orientation angle of β with the velocity direction. The resultant cutting force excites the flexibilities leading to vibrations in directions x_i . When the vibrations generated during the previous and current passes are projected into the direction of chip thickness (r), the

chatter type is considered to be regenerative and it is most commonly observed in production. Even if the previous pass is neglected, the vibrations at the current pass in two orthogonal directions affect the cutting forces which lead to the mode coupling chatter. The regenerative and mode coupling chatter mechanisms are presented first, followed by the process damping mechanism to consider the effect of the tool's flank contact with the wavy surface finish.

2.1 Chatter Stability Model in the Frequency Domain

The chip thickness $h(t)$ varies as a function of the present vibration amplitude $r(t)$ and vibrations left on the cut surface during the previous pass $r(t-T)$ [4, 5]:

$$h(t) = h_0 + h_d(t) = h_0 - [r(t) - r(t-T)], \quad (1)$$

where the delay T is the time between the two passes, h_0 is the commanded (static) chip thickness which corresponds to the feed per revolution in orthogonal turning (Figure 1a), and h_d is the dynamic (time-varying) chip thickness. The chip thickness ($h(t)$) produces variable tangential (F_t) and normal (F_r) cutting forces which form the resultant cutting force (F_c) as:

$$\begin{aligned} F_t(t) &= K_t ah(t), \quad F_r(t) = K_r F_t(t) = K_r K_t ah(t) \\ F_c(t) &= \sqrt{F_t^2(t) + F_r^2(t)} = K_c ah(t) \leftarrow K_c = K_t \sqrt{1 + K_r^2}, \end{aligned} \quad (2)$$

where K_t is the tangential cutting force coefficient, $K_r = F_r / F_t = \tan \beta$ is the radial to tangential force ratio, and a is the depth of cut. The edge components of the cutting forces, which depend only on the depth of cut, are neglected since they don't contribute to the regeneration of chip thickness. The cutting force coefficients are either identified from the orthogonal to oblique cutting transformation using Merchant's thin shear plane model [27, 28] or mechanistically evaluated from cutting tests by considering the chip thickness and thermal softening effects [29]. The resultant cutting force excites each spring i attached to the tool by projection into the corresponding mode's direction:

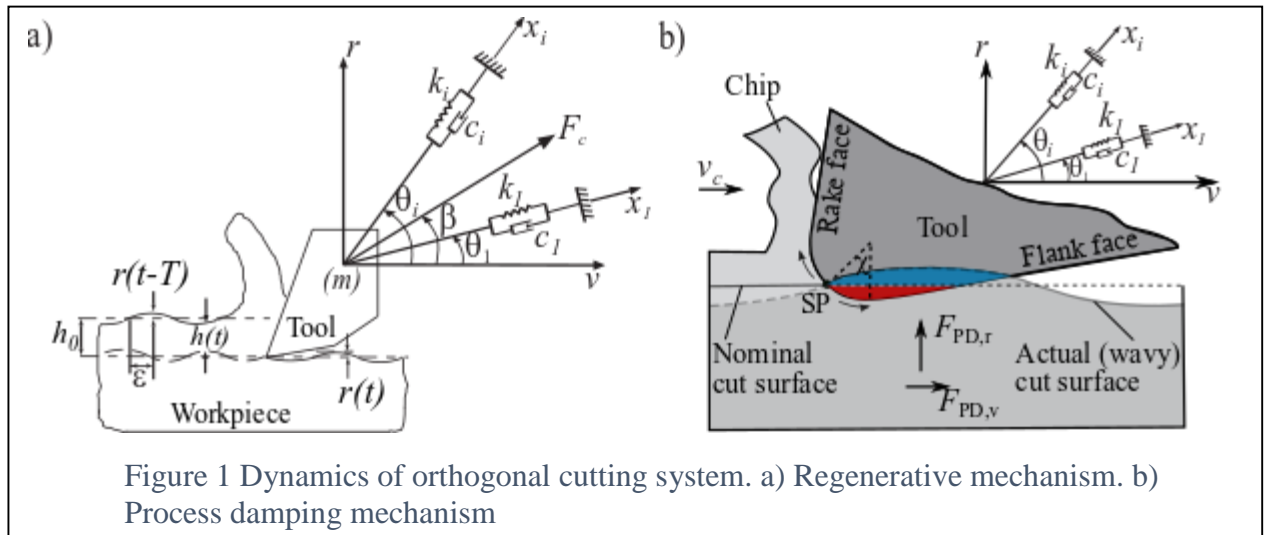


Figure 1 Dynamics of orthogonal cutting system. a) Regenerative mechanism. b) Process damping mechanism

$$F_i(t) = F_c(t) \cos(\theta_i - \beta). \quad (3)$$

Each mode with a transfer function of ($\Phi_{ii}(s)$) will cause vibration $x_i(s)$ in the Laplace domain (s) as:

$$x_i(s) = \Phi_{ii}(s) F_i(s). \quad (4)$$

By projecting and superposing all the vibrations in the chip thickness (r) direction, vibration in this direction is calculated according to:

$$r(s) = \Phi_o(s) F_c(s) \rightarrow \Phi_o(s) = \sum_{i=1}^l [\sin \theta_i \cos(\theta_i - \beta) \Phi_i(s)], \quad (5)$$

where $\Phi_o(s)$ is the oriented transfer function between the vibrations in the chip thickness and resultant cutting force directions. By neglecting the static chip thickness (h_0), which does not affect stability, the dynamic or regenerative chip thickness contributed by the vibrations is evaluated as:

$$h_d(t) = -\Delta r(t) = -[r(t) - r(t-T)], \quad (6)$$

where the time delay is $T = 60/n$ for the spindle speed n [rev/min]. Substituting the dynamic chip thickness into the resultant cutting force (Eq. (2)) yields the dynamic cutting force in the Laplace domain as:

$$F_c(s) = -K_c a \Delta r(s) = -K_c a (1 - e^{-sT}) \Phi_0(s) F_c(s). \quad (7)$$

The characteristic equation of the system is:

$$1 + K_c a (1 - e^{-sT}) \Phi_0(s) = 0, \quad (8)$$

which has an infinite number of roots due to the delay term e^{-sT} . By substituting $s = i\omega_c$ for the critical stability condition, the characteristic equation of the dynamic cutting system in the frequency domain becomes:

$$1 + \Lambda \Phi_0(i\omega_c) = 0 \rightarrow \Lambda = a K_c (1 - e^{-i\omega_c T}) = \frac{-1}{\Phi_0(i\omega_c)} = \frac{-1}{G_0(\omega_c) + i H_0(\omega_c)}, \quad (9)$$

where G_o and H_o are the real and imaginary parts of oriented frequency response function, or FRF (Φ_0). Expanding Eq. (9) gives:

$$\begin{aligned} \Lambda &= \frac{-1}{G_0(\omega_c) + i H_0(\omega_c)} = a K_c (1 - e^{-i\omega_c T}) = a K_c [(1 - \cos \omega_c T) + i \sin \omega_c T] \\ &\{1 + a K_c [G_0(1 - \cos \omega_c T) - H_0 \sin \omega_c T]\} + i a K_c \{G_0 \sin \omega_c T + H_0 (1 - \cos \omega_c T)\} = 0 \end{aligned} \quad (10)$$

and equating the imaginary part to zero leads to the critical spindle speed (n):

$$\begin{aligned}
G_0 \sin \omega_c T + H_0 (1 - \cos \omega_c T) &= 0 \rightarrow \tan \psi = \frac{H_0}{G_0} = \frac{\sin \omega_c T}{\cos \omega_c T - 1} \\
\tan \psi &= \tan \left[\frac{\omega_c T}{2} - 3 \frac{\pi}{2} \right] \rightarrow \omega_c T = 2\psi + 3\pi = (2k_l + 1)\pi + 2\psi \leftarrow k_l = 1, 2, \dots \\
\text{Speed: } n[\text{rev / min}] &= \frac{60}{T} = 60 \frac{\omega_c}{(2k_l + 1)\pi + 2\psi}
\end{aligned} \tag{11}$$

By also equating the real part to zero and substituting $H_0 / G_0 = \sin \omega_c T / (\cos \omega_c T - 1)$, the critical depth of cut a_{\lim} is determined to be:

$$a_{\lim} = \frac{-1}{K_c G_0(\omega_c) \left[(1 - \cos \omega_c T) - \frac{H_0(\omega_c)}{G_0(\omega_c)} \sin \omega_c T \right]} = \frac{-1}{2K_c G_0(\omega_c)}. \tag{12}$$

The solution leads to a positive depth of cut only when the real part of the oriented FRF ($G_0(\omega_c)$) is negative. Tobias considered the entire negative region of the real part of the FRF which leads to the critical depth of cut and corresponding spindle speeds for each integer number of vibration waves (k_l) generated within the time delay (i.e., spindle period) T that led to the *stability lobes* [4]. Tlusty considered the worst case by taking the minimum of $G_0(\omega_c)$ which led to the minimum depth of cut regardless of the spindle speed [5]:

$$a_{\min} = \frac{-1}{2K_c \left\{ \min G_0(\omega_c) \right\}}. \tag{13}$$

Case 1: Mode coupling with zero time delay ($r(t-T) = 0$)

The eigenvalue (Eq.(9)) in mode coupling does not contain the delay term and the system must have at least two flexibilities which affect the chip thickness through the excitation by the cutting force. Consider a case with two flexibilities which are orthogonal to each other, but oriented from the velocity and chip thickness directions, i.e. $\theta_2 = \theta_1 + \pi/2$. The characteristic equation (9) becomes:

$$\begin{aligned}
\Phi_o(s) &= \sin \theta_1 \cos(\theta_1 - \beta) \Phi_1(s) - \cos \theta_1 \sin(\theta_1 - \beta) \Phi_2(s) \\
1 + \Lambda \Phi_0(i\omega_c) &= 0 \rightarrow \Lambda = aK_c = \frac{-1}{G_0(\omega_c) + iH_0(\omega_c)} \\
a_{\lim} &= \frac{-1}{K_c [G_0(\omega_c) + iH_0(\omega_c)]}
\end{aligned}$$

Since a_{\lim} is a real number, the imaginary part of the oriented FRF must have a zero crossing, i.e., $H_0(\omega_{mc}) = 0$ at the mode coupling chatter frequency ω_{mc} . Mode coupling chatter is independent of speed and has the limiting depth of cut:

$$a_{\lim} = \frac{-1}{K_c G_0(\omega_{mc})}, \quad (14)$$

which leads to about two times more stable depth than regenerative chatter. The orientation of the cutting force and modes alter the stability as indicated by Eq. (14). If the imaginary part of the oriented FRF does not cross zero, mode coupling would not occur. Ismail *et al.* showed that the mode coupling stability can be improved by selecting the ratio of modes through the modification of end mill stiffness [30].

Case 2: Regenerative chatter stability with process damping

Consider that the system is flexible only in the chip direction (r) and the force is also in the same direction for simplicity to explain the process damping mechanism ($\theta = \pi/2, \beta = \pi/2$). The clearance face and edge radius of the tool have time-varying ploughing contact with the presently cut wavy surface (Figure 1b) which generates a damping force, $aC_p \dot{r}/v_c$, proportional to the process damping constant of the material ($C_p [N/m]$) and the ratio of the vibration velocity ($\dot{r} = dr/dt$) to the cutting speed (v_c) as described by Das and Tobias [31]. Assuming a structure with stiffness (k), a viscous damping coefficient (c), and a mass (m) with a corresponding natural frequency $\omega_n = \sqrt{k/m}$ and damping ratio $\zeta = c/(2\sqrt{km})$ is excited by the regenerative cutting and process damping forces, $F_r(t) = K_r K_t a h(t) - aC_p \dot{r}/v_c$, the equation of motion for orthogonal cutting is expressed as:

$$\ddot{r} + 2\zeta\omega_n \dot{r} + \omega_n^2 r = \frac{\omega_n^2}{k} F_r(t) = \frac{\omega_n^2}{k} \left[K_r K_t a h(t) - aC_p \frac{\dot{r}}{v_c} \right] \quad (15)$$

Note that the process damping term contains vibration velocity (\dot{r}), which increases the viscous damping of the system. Eq. (15) is expressed in the Laplace domain as:

$$\begin{aligned} \left[s^2 + 2\zeta\omega_n s + \omega_n^2 \right] r(s) &= \frac{\omega_n^2}{k} K_r K_t a \left[h_0 - (1 - e^{-sT}) r(s) \right] - \frac{\omega_n^2}{k} \frac{1}{v_c} C_p s r(s) \\ \Phi(s) &= \frac{r(s)}{F_r(s)} = \frac{\omega_n^2 / k}{s^2 + 2\zeta\omega_n s + \omega_n^2} \end{aligned} \quad (16)$$

where $\Phi(s)$ is the transfer function of the system's structural dynamics in the chip thickness direction. Eq. (16) was expressed as a closed-loop system by Merritt [12], but without the process damping term which is now included in Figure 2. The closed-loop transfer function of the system is expressed as:

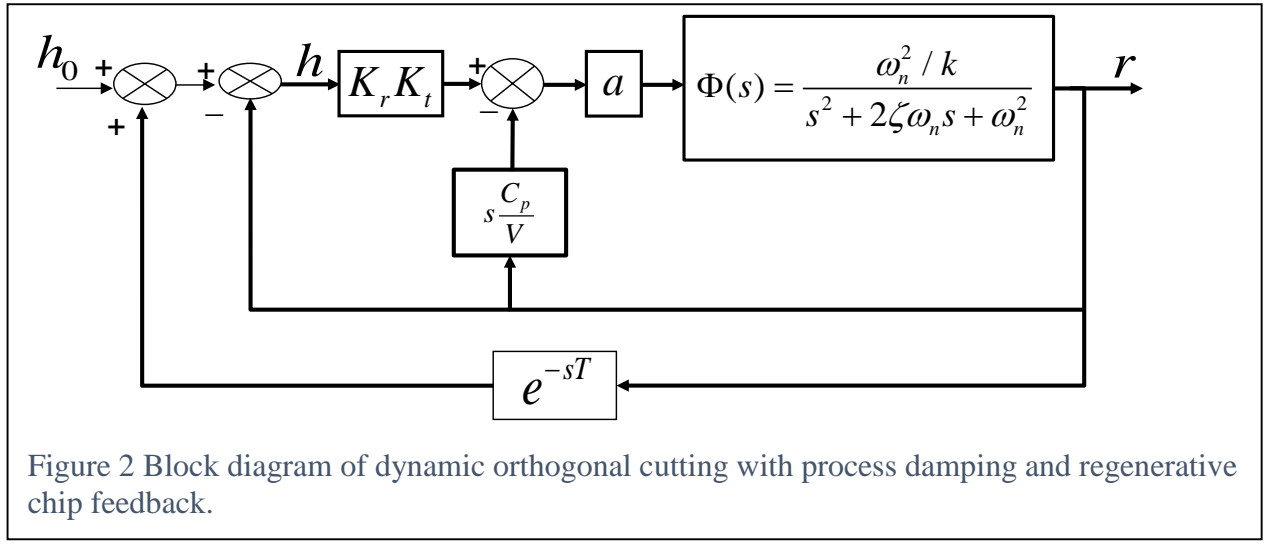


Figure 2 Block diagram of dynamic orthogonal cutting with process damping and regenerative chip feedback.

$$\frac{h(s)}{h_0(s)} = \frac{1 + a \frac{C_p}{v_c} \Phi(s)s}{1 + a \left[(1 - e^{-sT}) K_r K_t + \frac{C_p}{v_c} s \right] \Phi(s)}. \quad (17)$$

The characteristic equation of the system $\left(1 + a \left[(1 - e^{-sT}) K_t + (C_p / v_c) s \right] \Phi(s)\right)$ has an infinite number of roots ($s = \sigma \pm i\omega_c$) due to the delay term e^{-sT} . By considering the critical stability limit, where the real part of the root is zero ($\sigma = 0$) and the structure's FRF is represented by its real and imaginary parts ($[\Phi(i\omega_c) = G(\omega_c) + iH(\omega_c)]$), the characteristic equation becomes:

$$\left\{ 1 + K_r K_t a_{lim} \left[G(1 - \cos \omega_c T) - H \left(\sin \omega_c T - \frac{C_p}{v_c} \omega_c \right) \right] \right\} + i \left\{ K_r K_t a_{lim} \left[G \left(\sin \omega_c T + \frac{C_p}{v_c} \omega_c \right) + H(1 - \cos \omega_c T) \right] \right\} = 0. \quad (18)$$

Note that regardless of whether the system has a regenerative delay ($e^{-j\omega_c T}$) or not such as in mode coupling, the process damping affects the system dynamics as shown in Eq. (18). Tlusty *et al.* [5] and Tobias *et al.* [4] neglected the process damping term (i.e., $C_p = 0$) to find an analytical, frequency domain stability solution in their initial publications as described in Case 2. By forcing both the real and imaginary parts of Eq. (18) to zero, the critical depth of cut (a_{lim}) and spindle speed (n) are found by Tobias and Fishwick [4] as :

$$a_{lim}[m] = \frac{-1}{2K_r K_t G(\omega_c)}; n[rev/min] = 60 \frac{\omega_c}{(2k_l + 1)\pi + \psi} \leftarrow \psi = \tan^{-1} \frac{H(\omega_c)}{G(\omega_c)}, k_l = 0, 1, 2, \dots \quad (19)$$

The stability solution exists only when the real part of the FRF is negative [4], i.e., $G(\omega_c) < 0$. Since the negative real part has the smallest value near the natural frequency (ω_n) of the structure, the highest depth of cut is achieved when the spindle speed is close to the natural frequency (i.e., the first stability lobe $k_l = 0$) or at its integer (k_l) fractions or lobes [7]. Tlusty and Polacek [5] took the minimum negative real part of the FRF [5] as:

$$a_{\min} = \frac{-1}{2K_r K_t G_{\min}(\omega_c)} = \frac{2k\zeta}{K_r K_t} \leftarrow G_{\min}(\omega_c) \approx \frac{-1}{4k\zeta}, \quad (20)$$

which gives the absolute minimum depth of cut that is linearly proportional to the dynamic stiffness of the machine ($2k\zeta$) and inversely proportional to the product of the cutting force coefficients for the selected work material ($K_r K_t$). Tlusty's simple formula (Eq.(20)) has been widely used as a guide by machine tool designers and Tobias's formula has been applied to select the stable depth of cuts at high spindle speeds [7].

Sample stability lobes are shown for mode coupling, with and without the process damping effect,

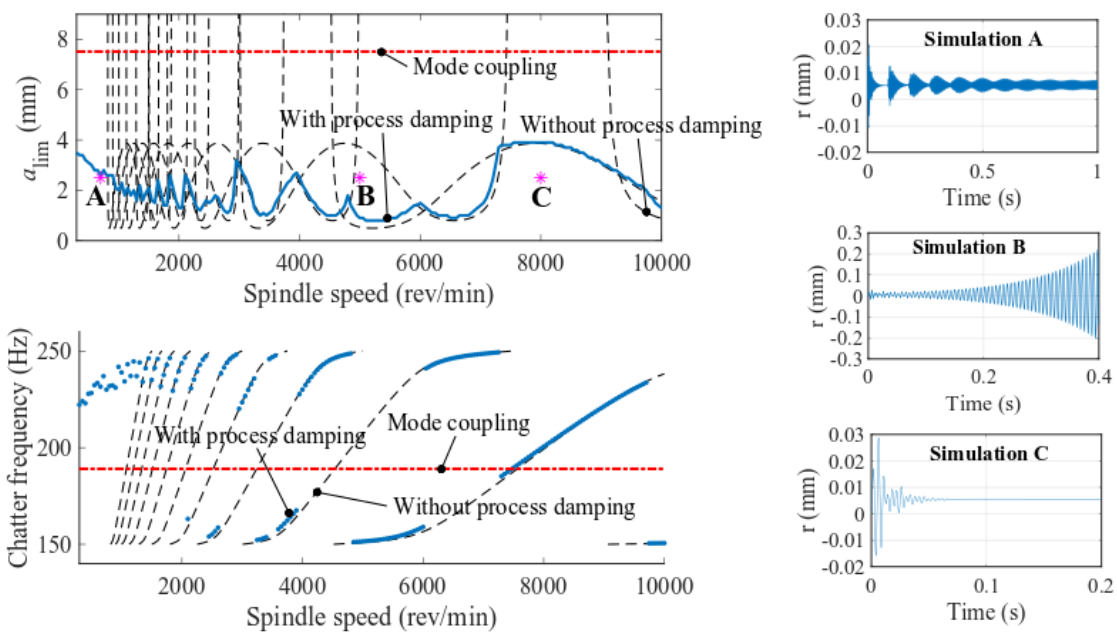


Figure 3 Chatter stability diagrams and corresponding chatter frequency diagram for mode coupling chatter, and regenerative chatter with and without process damping. Simulation parameters: Cutting coefficients - $K_t=1000$ MPa, $K_r=0.3$; Modal parameters- $k_1=15\times 10^6$ N/m, $k_2=10\times 10^6$ N/m, $\omega_{n,1}=150$ Hz, $\omega_{n,2}=250$ Hz, $\zeta_1=0.010$, $\zeta_2=0.012$. The orientation of flexibilities- $\theta_1=70$ deg, $\theta_2=160$ deg; process damping constant - $C_p=2e6$ N/m; workpiece diameter = 30 mm. Simulated cases: $h_0=0.1$ mm/rev, $a=2.5$ mm. Cases A: $n=700$ rev/min (stable, process damping zone), B: $n=5000$ rev/min (stable, high speed zone), C: $n=8000$ rev/min (unstable, high speed zone).

Figure 3. When the process damping is considered in Eq. (18), the spindle speed-dependent cutting velocity term (v_c) diverges from the solutions of Tobias (Eq.(19)) and Tlusty (Eq.(20)) at low cutting speeds. In this case, the critically stable depths of cut are first analytically solved without process damping. Later, the process damping is included and the depth of cut (a) at each speed (n) is increased until the critically stable condition is identified using the Nyquist stability criterion. The real and imaginary parts of the characteristics equation (Eq.(18)) are computed within the frequency range of the structure's FRF. The process is considered to be unstable if the polar plot of real and imaginary parts encircles the origin clockwise and is considered stable otherwise. If the polar plot passes through the origin, the process is critically stable at that particular speed and depth of cut [32, 33]. The process is repeated at each spindle speed to generate the stability lobes. Alternatively, the viscous damping term is modified by including the process damping term (i.e., $(2\zeta + aC_p / v_c)$), where the depth of cut (a) and speed (v_c) are adopted from the process damping free solution. The stability solution given in Eq. (19) is iteratively applied until the depth of cut converges to a critical limit [34]. The process damping constants are usually identified experimentally from cutting tests with or without chatter. With chatter [35], the constants are determined by considering the energy dissipation of the vibrations due to tool penetration into work material. The identification of process damping constants from chatter-free cutting tests is either based on the estimation of dynamic cutting forces contributed by the tool flank contact with the wavy surface [36] or the identification of equivalent damping ratios from the operational modal analysis [37]. Tuysuz and Altintas recently presented an analytical model of process damping based on contact mechanics laws [38].

2.2 Continuous time-domain analysis of turning

The stability analysis of stationary cutting processes can also be analyzed in the time domain using the state space approach from the classical mathematical theory of differential equations. Consider the governing equation of regenerative chatter for turning in the form of Eq.(15), where the cutting force and the flexibility are assumed to be only in the normal direction r as in Figure 1a. By neglecting the process damping term, the delay differential equation of the system becomes:

$$\ddot{r}(t) + 2\zeta\omega_n \dot{r}(t) + \omega_n^2 r(t) = \omega_n^2 \frac{K_r K_t}{k} a (h_0 + r(t-T) - r(t)), \quad (21)$$

which is further simplified using the dimensionless time to be:

$$\tilde{t} = \omega_n t, \quad \dot{r}(t) = \frac{d}{dt} r(t) = \omega_n \frac{d}{d\tilde{t}} r(\tilde{t}) = \omega_n r'(\tilde{t}), \quad \ddot{r}(t) = \omega_n^2 r''(\tilde{t}), \quad r(t-T) = r(\tilde{t}-\tilde{T}). \quad (22)$$

The dimensionless time delay \tilde{T} , spindle speed $\tilde{\Omega}$ and depth of cut \tilde{a} are defined as:

$$\tilde{T} = \omega_n T, \quad \tilde{\Omega} = \frac{2\pi}{\tilde{T}} = \frac{1}{\frac{\omega_n}{2\pi} T} = \frac{\Omega}{\omega_n} = \frac{n}{60f_n}, \quad \tilde{a} = \frac{K_r K_t}{k} a. \quad (23)$$

The spindle speed n is measured in [rev/min], so the angular velocity of the spindle is $f = n/60 = 1/T$ in [Hz], and it is $\Omega = 2\pi/T = 2\pi f$ in [rad/s], where the undamped natural

frequency $f_n = \omega_n / 2\pi$ is in [Hz]. The equation of motion (Eq.(21)) can be simplified for the small oscillation $\eta(\tilde{t}) = r(\tilde{t}) - r_0$ where the static deformation

$$r_0 = \frac{K_r K_t}{k} ah_0 = \tilde{a} h_0$$

of the tool causes a surface location error. The resulting governing equation then assumes the form

$$\eta''(\tilde{t}) + 2\zeta\eta'(\tilde{t}) + \eta(\tilde{t}) = \tilde{a}(\eta(\tilde{t} - \tilde{T}) - \eta(\tilde{t})), \quad (24)$$

where the three remaining parameters are: the damping ratio ζ , the dimensionless chip width \tilde{a} , and the dimensionless spindle speed $\tilde{\Omega}$:

$$\tilde{\Omega} = 2\pi / \tilde{T} = \Omega / \omega_n = f / f_n,$$

which is used to construct the stability charts in the parameter plane. The trial solution of the linear delay-differential equation is the same as it is for the linear ordinary differential equations:

$$\eta(\tilde{t}) = e^{\delta\tilde{t}} (A \cos(\omega\tilde{t}) + B \sin(\omega\tilde{t})). \quad (25)$$

Due to delay term, there are infinite values for δ and ω that satisfy Eq.(24). For the stability of stationary cutting, all the possible δ values must be negative for the exponentially decaying vibrations. The values of δ and ω correspond to the characteristic exponents $\lambda = \delta + i\omega$ in the Laplace domain, which corresponds to the Laplace transformation applied to Eq. (16) in the frequency domain with the relation $s = \lambda\omega_c$. Accordingly, the stability boundaries can be found in the $(\tilde{\Omega}, \tilde{a})$ plane when Eq. (25) is substituted back into Eq. (24) with $\delta=0$. The separation of the coefficients of the $\cos(\omega\tilde{t})$ and $\sin(\omega\tilde{t})$ terms leads to two equations for the dimensionless spindle speed $(\tilde{\Omega})$ and the dimensionless depth of cut \tilde{a} with the parameter ω . This ω can be interpreted as a dimensionless chatter frequency since it relates to the chatter frequency ω_c appearing in Eq. (18) according to $\omega = \omega_c / \omega_n = f_c / f_n$ along the stability boundaries when process damping is neglected. The corresponding closed-form expressions for the critically stable dimensionless spindle speed $(\tilde{\Omega})$ and depth of cut $((\tilde{a}))$ are:

$$\left. \begin{aligned} \tilde{\Omega} &= \frac{\omega}{k_l - \frac{1}{\pi} \arctan \frac{\omega^2 - 1}{2\zeta\omega}}, \quad k_l = 1, 2, \dots \\ \tilde{a} &= \frac{(\omega^2 - 1)^2 + 4\zeta^2\omega^2}{2(\omega^2 - 1)}, \quad 1 < \omega < \infty. \end{aligned} \right\} \quad (26)$$

These curves are also called stability lobes and they are presented in Figure 4 together with their characteristic parameters. The major characteristic parameters of the chart can be identified from Eq.(26). For example, the lower bound for all lobes is a straight-line at the absolute limit for the

depth of cut, below which the system is stable for any cutting speed. This value comes from Eq. (23) and Eq. (26):

$$a_{\min} = 2\zeta(1+\zeta) \frac{k}{K_r K_t} \approx \frac{2k\zeta}{K_r K_t}, \quad (27)$$

which is the same absolute minimum as given in Eq. (20) via the frequency domain model for small damping ratios. At these minimum parameter points of the lobes, the angular chatter frequency ω_c^* and the corresponding “worst” spindle speeds Ω^* are:

$$\omega_c^* = \sqrt{1+2\zeta} \omega_n \quad \text{and} \quad \Omega^* = \frac{\sqrt{1+2\zeta}}{k_l - \frac{1}{\pi} \arctan \frac{1}{\sqrt{1+2\zeta}}} \omega_n \approx \frac{4}{4k_l - 1} \omega_n, \quad k_l = 1, 2, \dots \quad (28)$$

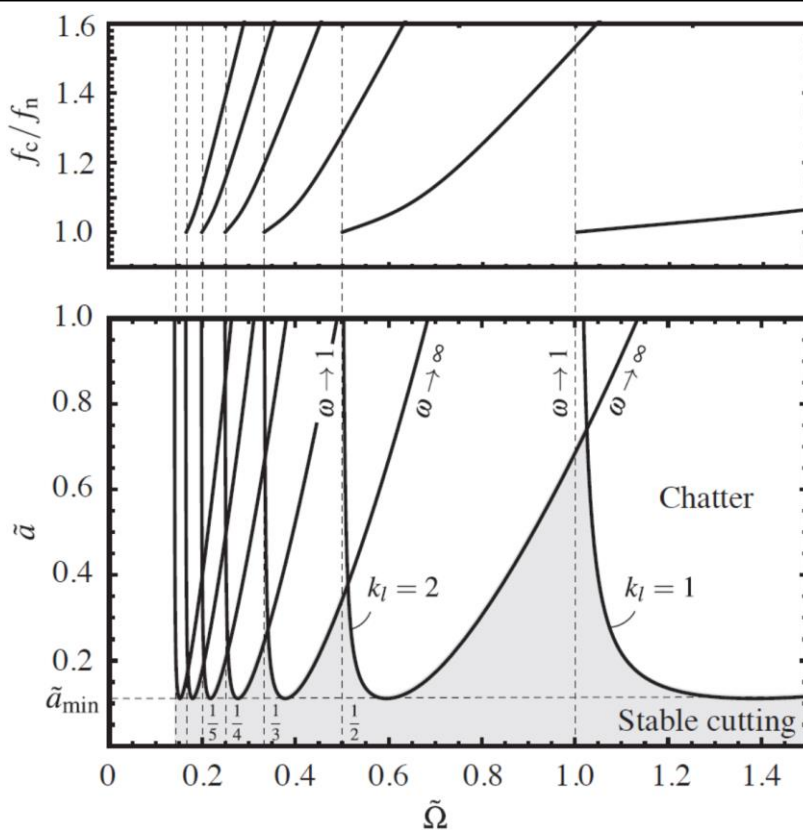


Figure 4. Theoretical stability chart of turning processes in the plane of the dimensionless spindle speed $\tilde{\Omega}$ and the dimensionless depth of cut \tilde{a} . The dimensionless chatter frequency $\omega = f_c / f_n$ is greater than 1. The damping ratio is fixed at $\zeta = 0.05$, while $k_l = 1, 2, \dots$ refers to the sequence number of the lobes.

while the stable pockets between the instability lobes can be reached close to the asymptotes of the lobes at the spindle speeds $\Omega^0 \approx \omega_n / k_l$, ($k_l = 1, 2, \dots$) where the expected chatter frequency is close to $\omega_c^0 \approx \omega_n$. Note that at the intersection of the lobes, quasi-periodic chatter may also occur with two frequencies involved. The dimensionless stability model in the time domain provides the critical speeds where the depths of cut are either maximum or minimum as a function of the natural frequency of the structure.

2.3 Discrete time-domain analysis of highly interrupted cutting

As opposed to the continuous time domain analysis, the discrete time-domain analysis can also be represented in case of the simplified model of highly interrupted orthogonal cutting shown in *Figure 5*. Consider the mechanical model of the regenerative mechanism introduced in Figure 1, where only one vibration mode is relevant at the angle $\theta_i = \pi/2$, so the tool position is given by the single coordinate $x := x_i = r$. The cylindrical workpiece has a rotation period T , which means that its circumference is Tv_c , where v_c is the cutting speed. However, the cylindrical workpiece has a large groove of width $(1 - \rho)Tv_c$, and it is hypothetically assumed that this groove is almost as large as the whole circumference of the workpiece. The tool is therefore in cut for only very short time intervals $\rho T \rightarrow 0$, where the dimensionless parameter ρ stands for the ratio of the time spent in the cut to the time spent out of the cut. The depth of cut is still a , so during this very short time of contact, the tool is subjected to a kind of impact load due to the cutting force applied during the very short contact time ρT . Still, the regenerative mechanism appears again, since the impact force will depend on the difference of the past and present positions of the tool during contact.

Note, that the same mechanical model can also be derived from the dynamics of milling presented in Section 3 (see Figure 7). In that case, the rotating tool is considered to be rigid in the y direction and flexible only in the x direction. Assume that the milling tool has only one cutting edge with rotation period T , the cutting speed is v_c again, and the circumference of the milling tool is Tv_c .

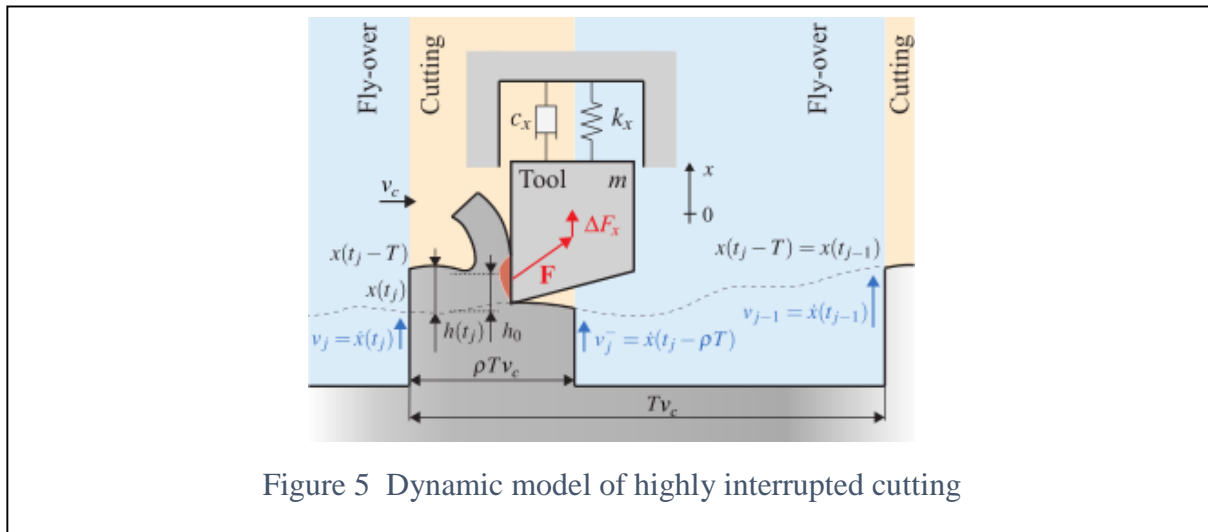


Figure 5 Dynamic model of highly interrupted cutting

Now, the workpiece is assumed to be thin with a thickness of $\rho T v_c$ in the cutting speed direction. If the single cut at each rotation takes place at $\phi_l = \pi/2$ only, the dynamic model of milling is simplified to the one shown in Figure 5.

For these simplified conditions, the process can be solved analytically in the time domain and a discrete time mathematical model can be constructed to determine an analytical stability chart having a structure similar to the turning stability chart shown in Figure 4. This procedure applies the time domain solution of the fly-over section as a lightly damped oscillator, while the short cutting response is calculated according to the Newtonian impact theory: the position of the tool does not change during this short cutting period, while the velocity of the tool changes abruptly due to the impulse-like cutting force.

In accordance with the notation in *Figure 5*, consider that the tool leaves the workpiece at time instants $t_j = jT$, $j = 0, 1, 2, \dots$. At the $(j-1)^{\text{st}}$ time instant, the tool starts a free-flight with the initial position $x_{j-1} = x(t_{j-1}) = x(t_j - T)$ and the initial velocity $v_{j-1} = \dot{x}(t_{j-1}) = \dot{x}(t_j - T)$. The tool has a damped angular natural frequency $\omega_d = \omega_n \sqrt{1 - \zeta^2}$. The homogeneous ordinary differential equation of the system during free-flight (i.e., free vibration with some initial conditions) is:

$$\ddot{x}(t) + 2\zeta\omega_n\dot{x}(t) + \omega_n^2x(t) = 0 \quad (29)$$

with the following solution

$$\left. \begin{aligned} x(t) &= \left(\frac{e^{-\zeta\omega_n t}}{\sqrt{1-\zeta^2}} \cos(\omega_d t - \varepsilon) \right) x_{j-1} + \left(\frac{e^{-\zeta\omega_n t}}{\omega_d} \sin(\omega_d t) \right) v_{j-1} \\ \dot{x}(t) &= \left(-\frac{\omega_n e^{-\zeta\omega_n t}}{\sqrt{1-\zeta^2}} \sin(\omega_d t) \right) x_{j-1} + \left(\frac{e^{-\zeta\omega_n t}}{\sqrt{1-\zeta^2}} \cos(\omega_d t + \varepsilon) \right) v_{j-1} \end{aligned} \right\} v_i^- = \dot{x}((1-\rho)T) \approx \dot{x}(T), \quad (30)$$

where the phase angle ε is calculated from $\tan \varepsilon = \zeta / \sqrt{1 - \zeta^2}$. The position and the velocity of the tool can then be calculated when it enters the workpiece again by substituting $t = (1 - \rho)T \approx T$ into Eq. (30) :

$$v_i^- = \dot{x}((1-\rho)T) \approx \dot{x}(T), \quad (31)$$

where the negative sign in the superscript refers to the fact that these values occur at the start of the short impact-like cutting. During this infinitesimally short cutting time of ρT , the variation of the position of the tool is negligible, while the cutting force variation $\Delta F_r = K_r K_t a(x_{j-1} - x_j)$ has the linear impulse that causes the variation $m(v_j - v_i^-)$ of the tool's linear momentum. Accordingly, when the tool leaves the workpiece again at the time instant t_j , its position and the velocity can be calculated as:

$$\left. \begin{aligned} x_j &\approx x_j^- \approx x(T) \\ v_j = v_j^- + \omega_n^2 \frac{K_r K_t}{k_x} a(x_{j-1} - x_j) \rho T &\approx \dot{x}(T) + \rho T \frac{K_r K_t}{k_x} a \omega_n^2 (x(0) - x(T)) \end{aligned} \right\} \quad (32)$$

Substituting the values of $x(0)$ and $x(T)$ from Eq. (30), a discrete time model is obtained that describes the connection of the subsequent positions and velocities of the tool after each short cutting period by means of the two-dimensional iteration:

$$\begin{pmatrix} x_j \\ v_j \end{pmatrix} = \begin{pmatrix} A_{11} & A_{12} \\ A_{21} & A_{22} \end{pmatrix} \begin{pmatrix} x_{j-1} \\ v_{j-1} \end{pmatrix}, \quad j=1, 2, \dots \quad (33)$$

where

$$\begin{aligned} A_{11} &= \frac{e^{-\zeta \omega_n T}}{\sqrt{1-\zeta^2}} \cos(\omega_d T - \varepsilon), \quad A_{12} = \frac{e^{-\zeta \omega_n T}}{\omega_d} \sin(\omega_d T) \\ A_{21} &= -\frac{\omega_n e^{-\zeta \omega_n T}}{\sqrt{1-\zeta^2}} \sin(\omega_d T) + \rho T \omega_n^2 \left(\frac{K_r K_t}{k_x} a \right) \left(1 - \frac{e^{-\zeta T}}{\sqrt{1-\zeta^2}} \cos(\omega_d T - \varepsilon) \right) \\ A_{22} &= \frac{e^{-\zeta \omega_n T}}{\sqrt{1-\zeta^2}} \left(\cos(\omega_d T + \varepsilon) - \rho T \omega_n \left(\frac{K_r K_t}{k_x} a \right) \sin(\omega_d T) \right). \end{aligned}$$

The stability of the stationary highly interrupted cutting process is equivalent to the convergence of the geometric vector series given in Eq.(33), which means that the quotients, $\mu_{1,2}$, that is, the eigenvalues of the quotient matrix \mathbf{A} in Eq.(33), must have moduli less than 1: $|\mu_{1,2}| < 1$.

In this discrete system (Eq.(33)), the counterpart of the classical chatter with angular frequency ω_c appears when the following characteristic equation has the complex conjugate roots $\mu_{1,2} = e^{i\omega_c} = \cos \omega_c + i \sin \omega_c$ on the unit circle of the complex plane which satisfy:

$$\det(\mu \mathbf{I} - \mathbf{A}) = \mu^2 - (A_{11} + A_{22})\mu + (A_{11}A_{22} - A_{12}A_{21}) = 0. \quad (34)$$

Using the same dimensionless quantities as defined in Eq.(23), the substitution of these roots into Eq. (34) leads to the chatter boundaries \tilde{a}_c for the dimensionless axial depth of cut in the following explicit form:

$$\tilde{a}_c = -\frac{\tilde{\Omega} \sqrt{1-\zeta^2}}{\rho \pi} \cdot \frac{\sinh\left(\zeta \frac{2\pi}{\tilde{\Omega}}\right)}{\sin\left(\sqrt{1-\zeta^2} \frac{2\pi}{\tilde{\Omega}}\right)} > \tilde{a}_{c,\min} = \frac{2\zeta \sqrt{1-\zeta^2}}{\rho}, \quad (35)$$

where the lower estimate for the absolute stable region is not as sharp as it is in case of turning, but the formula is quite good in the high spindle speed domain as shown in Figure 6. However, there appears another kind of vibration that does not occur in turning. This is the result of a period-doubling (or period-2) bifurcation, when the critical characteristic root is $\mu_1 = -1$, while $|\mu_2| < 1$. It is called period-doubling because the corresponding time period of the critical chatter vibration

is two times the time period of the spindle rotation. If this is substituted back into Eq. (34), the new kind of instability lobes have the following closed-form expression:

$$\tilde{a}_{pd} = \frac{\tilde{\Omega}\sqrt{1-\zeta^2}}{2\pi\rho} \cdot \frac{\cos\left(\sqrt{1-\zeta^2} \frac{2\pi}{\tilde{\Omega}}\right) + \cosh\left(\zeta \frac{2\pi}{\tilde{\Omega}}\right)}{\sin\left(\sqrt{1-\zeta^2} \frac{2\pi}{\tilde{\Omega}}\right)} > \tilde{a}_{pd,min} = \frac{\zeta\sqrt{1-\zeta^2}}{\rho}. \quad (36)$$

These stability boundaries are presented in Figure 6. Compared to the stability chart of turning in Figure 4, the number of lobes is doubled, the classical chatter lobes become much thinner and, although the period-doubling lobes show up between them, large stable pockets are still present at $\tilde{\Omega} = 1/k_l$ similar to the case of turning. These stable pockets are relevant at high spindle speeds.

The chatter and period-doubling vibrations at the stability limits have a rich frequency content due to the parametric excitation in the time-delayed system. This means that the critical self-excited vibrations are not harmonic anymore, although they are periodic, and they still have a relevant fundamental harmonic vibration component. The corresponding dominant frequency is usually the lowest frequency among the many frequencies presented above the stability chart in Figure 6, but

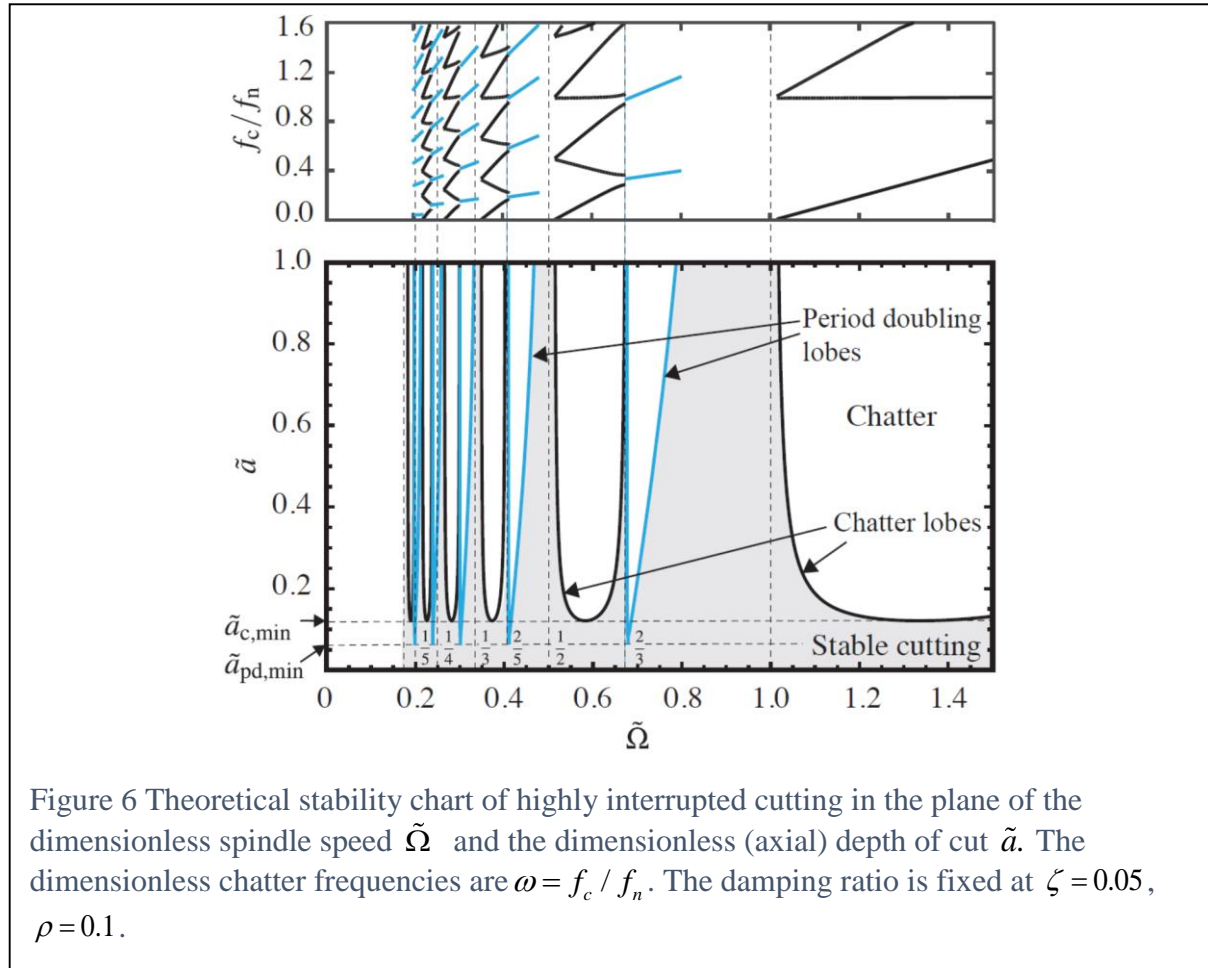


Figure 6 Theoretical stability chart of highly interrupted cutting in the plane of the dimensionless spindle speed $\tilde{\Omega}$ and the dimensionless (axial) depth of cut \tilde{a} . The dimensionless chatter frequencies are $\omega = f_c / f_n$. The damping ratio is fixed at $\zeta = 0.05$, $\rho = 0.1$.

not necessarily. Dombovari *et al.* [39] presented a simple method to identify the dominant chatter frequency among the many harmonics.

This stability chart was constructed by Davies *et al.* [40, 41], and parallel to their work, by Budak *et al.* [22] and Merdol *et al.* [42] with the multi-frequency method, by Insperger *et al.* [26] using the semi-discretization method, and by Bayly *et al.* [43] using the time finite element method. The experimental verification of this double-lobe structure together with the precise identification of the rich chatter and period doubling frequencies including the relevant higher harmonics was given, for example, by Insperger *et al.* [44], Mann *et al.* [45], and by Gradisek *et al.* [46].

The stability chart in Figure 6 is valid for the extreme conditions of highly interrupted cutting, but it also provides the basic structure of the stability domains in milling processes especially for high-speed milling with a low number of cutting edges and with low radial immersion. Still, the precise determination of the lobe structure for general milling processes requires more sophisticated numerical tools like the one presented in Section 3.2 where the continuous and discrete time-domain analyses of Sections 2.2 and 2.3 are combined.

3. Chatter Stability in Multi-Point Machining

Multi-point machining operations, such as milling, are carried out with tools having multiple teeth that periodically cut the material. The dynamics and stability of milling operations are summarized in the following sections.

3.1 Stability of milling operations in the frequency domain

Milling cutters have multiple teeth that have intermittent engagements with the workpiece. A diagram of milling with dynamic flexibilities in feed (x) and normal (y) directions is shown in Figure 7. If the tooth j is at the angular immersion (ϕ_j) which is measured clockwise from the (y) axis, the dynamic chip thickness in the radial direction is generated by the vibrations at the present and previous tooth periods ($\Delta x(t) = x(t) - x(t-T)$, $\Delta y(t) = y(t) - y(t-T)$) as:

$$h_{dj}(t) = \Delta x(t) \sin \phi_j + \Delta y(t) \cos \phi_j. \quad (37)$$

The dynamic chip creates tangential ($F_{tj} = K_t a h(\phi_j)$) and radial ($F_{rj}(\phi_j) = K_r F_{tj}$) cutting forces at each engaged tooth, which are projected in the feed (x) and normal (y) directions, and they are summed to find the total force components exciting the structure [24].

$$\begin{Bmatrix} F_x(t) \\ F_y(t) \end{Bmatrix} = \frac{1}{2} a K_t \begin{bmatrix} a_{xx} & a_{xy} \\ a_{yx} & a_{yy} \end{bmatrix} \begin{Bmatrix} \Delta x(t) \\ \Delta y(t) \end{Bmatrix} \rightarrow \mathbf{F}(t) = \frac{1}{2} a K_t \mathbf{A}(t) \Delta(t) \quad (38)$$

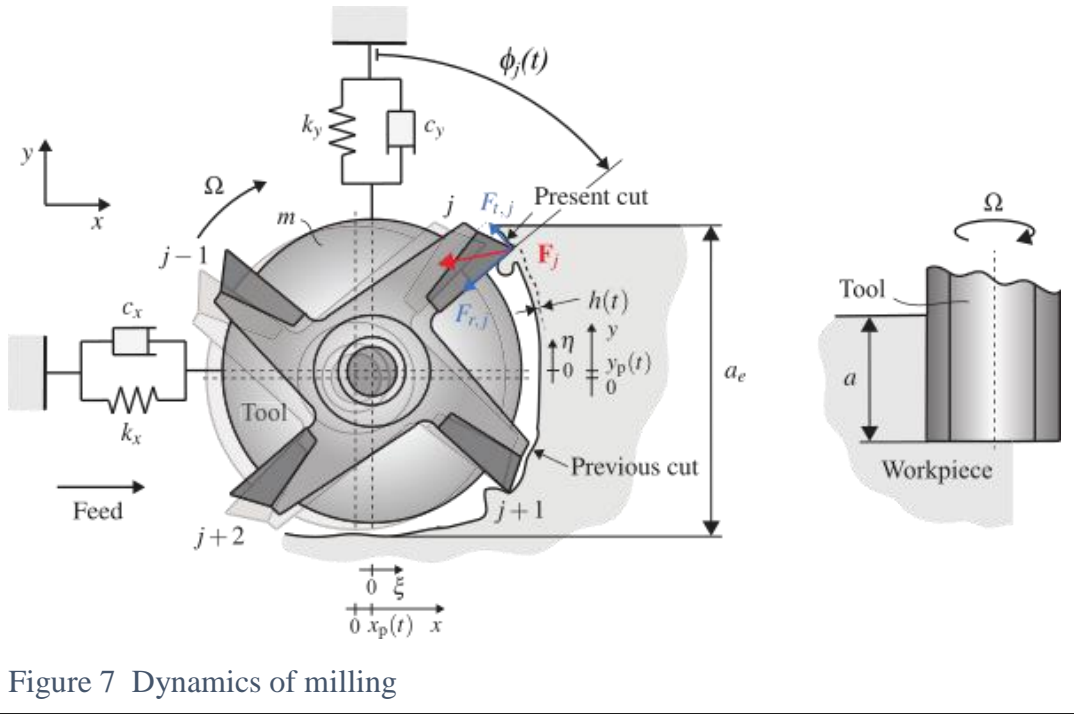


Figure 7 Dynamics of milling

The directional factors, which exist when the cutter is engaged with the workpiece (i.e., when a tooth is located between the start ϕ_{st} and exit ϕ_{ex} angles), are:

$$a_{xx} = \sum_{j=0}^{N-1} -g_j [\sin 2\phi_j + K_r (1 - \cos 2\phi_j)] ; \quad a_{xy} = \sum_{j=0}^{N-1} -g_j [(1 + \cos 2\phi_j) + K_r \sin 2\phi_j] \\ a_{yx} = \sum_{j=0}^{N-1} g_j [(1 - \cos 2\phi_j) - K_r \sin 2\phi_j] ; \quad a_{yy} = \sum_{j=0}^{N-1} g_j [\sin 2\phi_j - K_r (1 + \cos 2\phi_j)] \\ g_j = 1 \leftarrow \phi_{st} \leq \phi_j \leq \phi_{ex} \text{ and } g_j = 0 \text{ otherwise}$$

Since the cutter rotates at angular speed $\Omega(\text{rad} / \text{s})$, the immersion angle is time-varying ($\phi_j = \Omega t + (j-1)\phi_p \leftarrow \phi_p = 2\pi / N$). Consequently, the directional factors ($\mathbf{A}(t)$) are also time-varying and periodic at the tooth passing interval (T), or at the tooth passing frequency ($\omega_r = 2\pi / T$) in the frequency domain, or at cutter pitch angle intervals ($\phi_p = \Omega T = 2\pi / N$) in the angular domain. The periodic, dynamic cutting force (Eq.(38)) can be transformed into the frequency domain as:

$$\mathbf{F}(\omega) = \frac{1}{2} a K_t [\mathbf{A}(\omega) (1 - e^{-i\omega_c T}) \mathbf{q}(\omega)] \leftarrow \mathbf{q}(\omega) = \{x(\omega) \quad y(\omega)\}^T = \boldsymbol{\Phi}(i\omega) \mathbf{F}(\omega), \quad (39)$$

where $\boldsymbol{\Phi}(j\omega)$ is the FRF matrix of the structure in the $(xx, xy; yx, yy)$ directions. The periodic directional factors can be represented by their Fourier series components as [22]:

$$\mathbf{A}(\omega) = \sum_{r=-\infty}^{+\infty} \mathbf{A}_r e^{-ir\omega_r t} ; \quad \mathbf{A}_r = \frac{N}{2\pi} \int_{\phi_{st}}^{\phi_{ex}} \begin{bmatrix} a_{xx} & a_{xy} \\ a_{yx} & a_{yy} \end{bmatrix} e^{-irN\phi} d\phi, \quad (40)$$

where N is the number of teeth on the uniform pitch cutter. The details of transformations can be found in [33]. The resulting dynamic force for the milling system is expressed as [19]:

$$\mathbf{F}(\omega) = \frac{1}{2} a K_t [\mathbf{A}(\omega)(1 - e^{-i\omega_c T}) \boldsymbol{\Phi}(i\omega) \mathbf{F}(\omega)] \quad (41)$$

The stability condition provided in Eq. (41) is challenging to determine due to the presence of the delay term $e^{-i\omega_c T}$ and the corresponding periodicity of the directional matrix $\mathbf{A}(\omega)$ at the unknown tooth passing frequency ω_T . Minis and Yanushevsky [21] applied the Floquet theory to identify the critical stable depth of cut (a_{lim}) and spindle speed (n) iteratively. Budak and Altintas proposed two approaches: the zero-order solution [24], where only the average of directional factors is considered; and the multi-frequency [22] solution, which includes the harmonics of the directional factors for low immersion, highly intermittent milling operations.

Zero-Order Solution: In this case, only the average component of the directional matrix is considered so that [24]:

$$\mathbf{A}_0 = \frac{N}{2\pi} \int_{\phi_s}^{\phi_e} \begin{bmatrix} a_{xx} & a_{xy} \\ a_{yx} & a_{yy} \end{bmatrix} d\phi. \quad (42)$$

The dynamic milling (Eq. (41)) process then becomes time-invariant and its critical stability can be found from the characteristic equation using:

$$\Lambda = \Lambda_R + i\Lambda_I = -\frac{1}{2} K_t a (1 - e^{-i\omega_c T}) \rightarrow \det |I + \Lambda \mathbf{A}_0 \boldsymbol{\Phi}(i\omega)| = 0 \rightarrow a_0 \Lambda^2 + a_1 \Lambda + 1 = 0. \quad (43)$$

From the computed real (Λ_R) and imaginary (Λ_I) parts of the eigenvalues, the critical stable depth of cut (a_{lim}) and spindle speed (n) are evaluated directly as [24]:

$$a_{\text{lim}} = -\frac{2\pi\Lambda_R}{NK_t} [1 + \kappa^2] \leftarrow \kappa = \frac{\Lambda_I}{\Lambda_R} \quad (44)$$

$$T(\text{sec}) = \frac{\pi - 2 \tan^{-1} \kappa + k_l 2\pi}{\omega_c}, \quad n(\text{rev/min}) = \frac{60}{NT}, \quad k_l = 0, 1, 2, \dots$$

The analytical stability solution given in Eq. (44) is computationally inexpensive and sufficiently accurate for most of the common milling operations found in the industry. A comparison of experimentally validated stability lobes for the zero-order solution and time marching, numerical simulations are shown in Figure 8 [33]. While the numerical method, which is used as an accurate reference simulation, took more than 24 hours on a PC in 1997, the zero-order solution took less than a second because it is a direct, analytical solution.

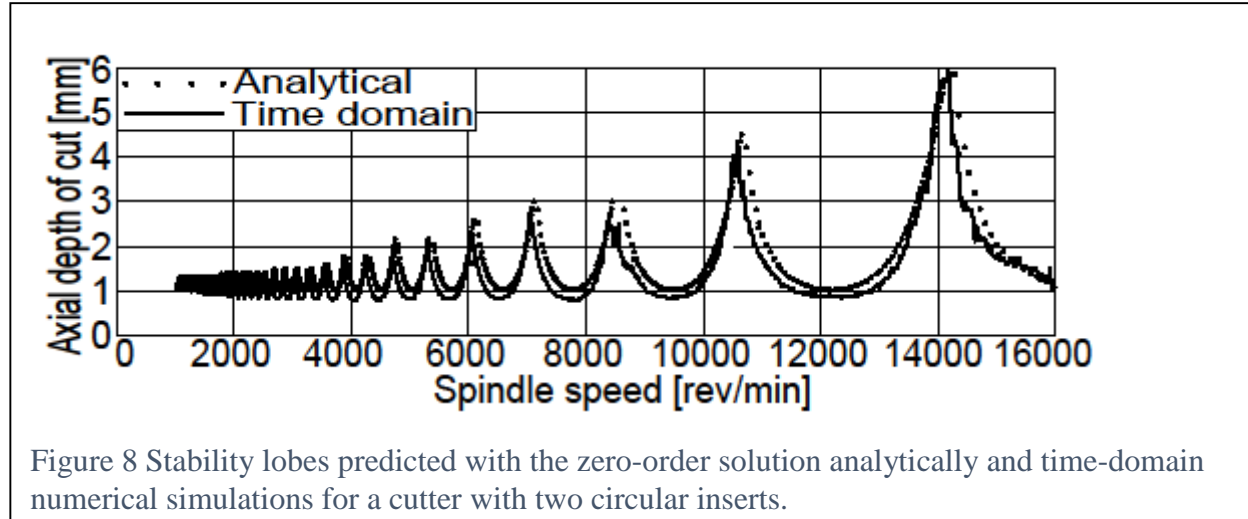


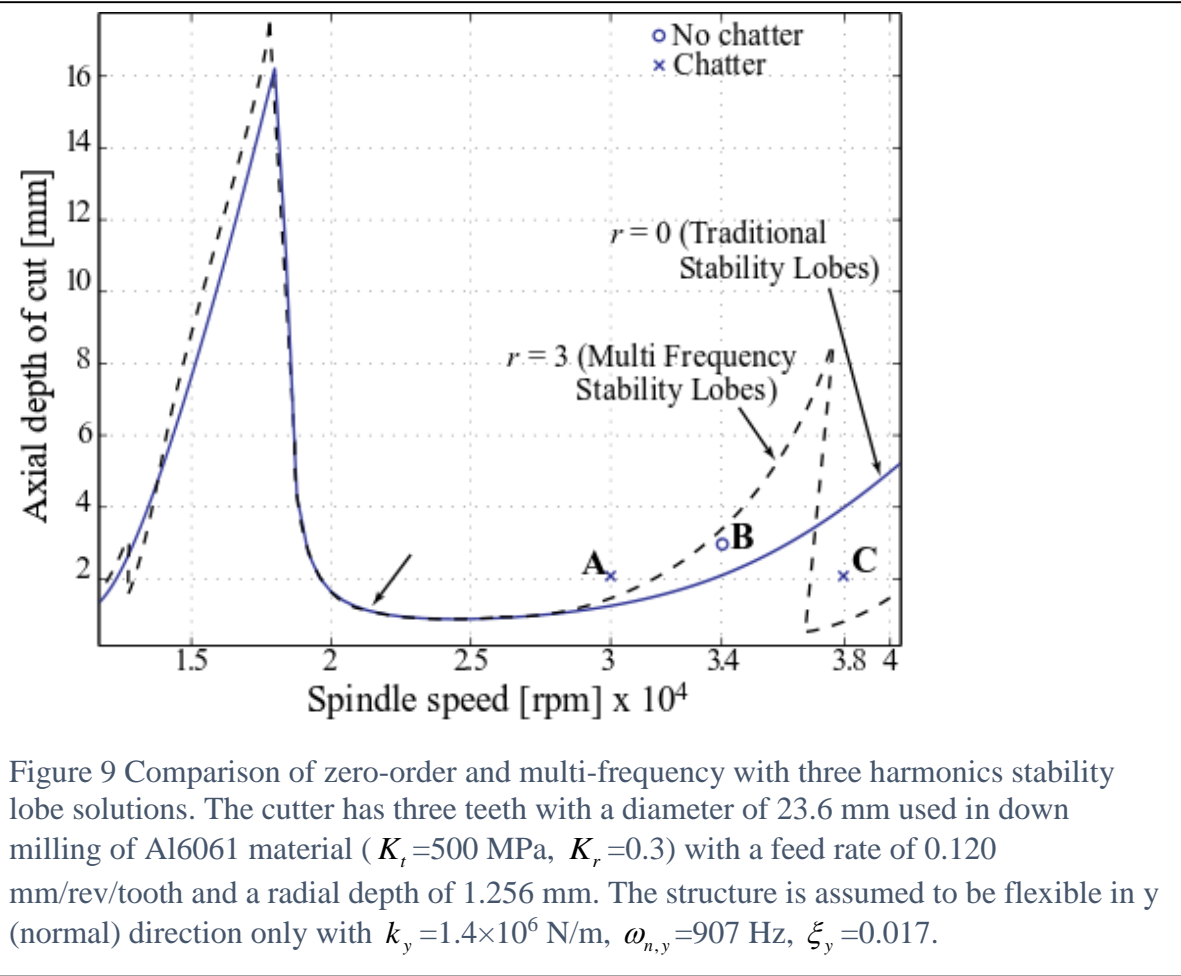
Figure 8 Stability lobes predicted with the zero-order solution analytically and time-domain numerical simulations for a cutter with two circular inserts.

Multi-Frequency Solution: When the harmonics of tooth passing frequency are included in the directional matrix $\mathbf{A}(\omega)$, the dynamic milling equation (Eq. (39)) is expanded using Floquet theory to obtain [22]:

$$\begin{aligned}\{\mathbf{F}(\omega)\} &= \sum_{l=-\infty}^{+\infty} \{\mathbf{P}_l\} \times \delta[\omega - (\omega_c + l\omega_T)] \\ \{\mathbf{F}(\omega)\} &= \Lambda \left\{ \sum_{r=-\infty}^{+\infty} \sum_{l=-\infty}^{\infty} [\mathbf{A}_{r-l}] [\Phi(\omega_c + l\omega_T)] \{\mathbf{F}(\omega)\} \right\} \leftarrow \Lambda = \frac{1}{2} a K_t (1 - e^{-i\omega_c T})\end{aligned}\quad (45)$$

This system has an infinite dimension, but it is truncated to few harmonics in practice. If the intermittency is severe, such as the case for small radial depths of cut, more harmonics of the tooth passing frequency (ω_T) need to be considered to obtain accurate results, which increases the size of the eigenvalue problem. For example, if only one harmonic is used ($(r, l) \in (0, \pm 1)$), the eigenvalue problem becomes:

$$\begin{Bmatrix} \{P_0\} \\ \{P_{-1}\} \\ \{P_1\} \end{Bmatrix}_{(6 \times 1)} = \Lambda \begin{pmatrix} [A_0] & [A_1] & [A_{-1}] \\ [A_{-1}] & [A_0] & [A_{-2}] \\ [A_1] & [A_{-2}] & [A_0] \end{pmatrix}_{(6 \times 6)} \begin{Bmatrix} [\Phi(\omega_c)] \\ [\Phi(\omega_c - \omega_T)] \\ [\Phi(\omega_c + \omega_T)] \end{Bmatrix}_{(6 \times 2)} \begin{Bmatrix} \{P_0\} \\ \{P_{-1}\} \\ \{P_1\} \end{Bmatrix}_{(6 \times 1)} \quad (46)$$



which leads to six eigenvalues and the eigenvalue that gives the minimum depth of cut is selected as a solution. Since the spindle speed is needed to find the tooth passing frequency (ω_T), the solution is obtained at each given spindle speed. Typically, even with the most severe intermittent conditions, including two to three harmonics is sufficient for stability convergence. The multi-frequency method is able to predict the added stability pockets (i.e., period-doubling lobes) at very high spindle speeds which are beyond the natural frequency of the structure; see Figure 9 [42]. An efficient elimination of false eigenvalues, which improves the computational speed, was developed by Merdol [33, 47].

3.2 Semi-discrete time-domain stability of milling operations

In the case of industrially realistic milling models, the milling tool has $N \geq 2$ cutting edges and the radial depth of cut is not negligible as it was assumed among the approximations of highly interrupted cutting in Section 2.3. Consequently, the analytical calculation of the lobe structure is no longer feasible. Even if a single vibration mode is considered in the x direction only as it was for the highly interrupted cutting model, the structure of the governing equation is:

$$\ddot{x}(t) + 2\zeta\omega_n \dot{x}(t) + \omega_n^2 x(t) = \omega_n^2 \frac{K_x A(t)}{k_x} a(x(t-T) - x(t)), \quad (47)$$

where the time delay is the tooth passing period $T = 2\pi/(N\Omega)$, and the directional factor $A(t) = A(t+T)$ is time-periodic with the same time period T as the delay (for details, see Section 3.1).

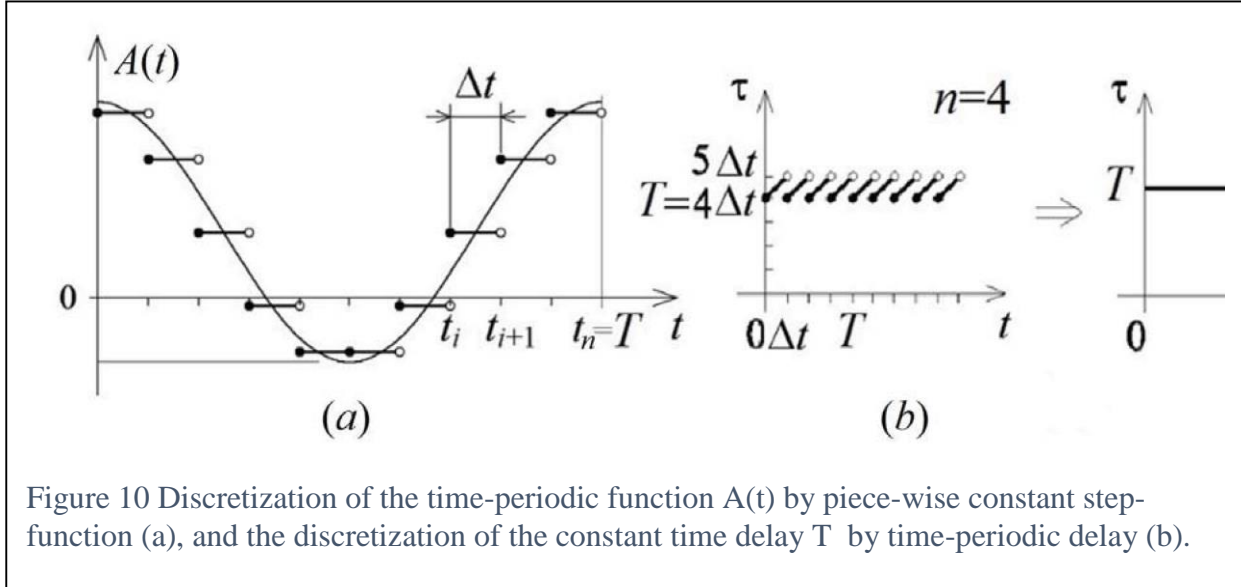


Figure 10 Discretization of the time-periodic function $A(t)$ by piece-wise constant step-function (a), and the discretization of the constant time delay T by time-periodic delay (b).

In this case, full discretization may be applied, where the time-periodic coefficients and the time derivatives are all discretized with discrete time intervals. This brute force method is successful, but, as explained in Section 2.2, the construction of a stability chart takes several hours on a standard personal computer. However, the combination of the continuous and discrete-time domain methods explained in Sections 2.2 and 2.3, respectively, results in a numerical method where the time derivatives are not discretized, but only the time periodicity and the time delay are. The basic idea of the discretization of the delay is not trivial. However, a discrete-time mapping can be constructed similar to the quotient matrix \mathbf{A} of highly interrupted cutting, but with a much larger size. The elements of the matrix can be calculated for each time step in closed form; analytical solutions of linear non-homogeneous ordinary differential equations can be used; and the computation time of the stability analysis can be reduced radically. Then, the stability boundaries can be reconstructed in the same way as in the case of Eq.(33). Although the size of the quotient matrix \mathbf{A} is large, there are several advanced and efficient numerical methods and related routines to check whether all eigenvalues of a large matrix have moduli less than 1.

The basic semi-discretization is now introduced. While it is straightforward to approximate the time-periodic function $A(t)$ in Eq.(47) by the piecewise constant function:

$$A(t) \approx A(i\Delta t) \text{ for } t \in [i\Delta t, (i+1)\Delta t), \quad i = 0, 1, \dots, (n-1), \quad (48)$$

where the discrete time step is $\Delta t = T/n$; see Figure 10a. It is more completed with respect to the time delay to obtain an approximate system in an analytically manageable system of linear

ordinary differential equations. The corresponding discretization of the time delay is represented graphically in Figure 10b, where a specific time-periodic delay:

$$\tau(t) = t + (n - \text{int}(t / \Delta t))\Delta t \quad (49)$$

is defined that refers back to the same time instant in the past for each time step:

$$x(t-T) \approx x(t-\tau(t)) = x(t-(t-(n-\text{int}(t/\Delta t))\Delta t)) = x(j\Delta t-T) = x((j-n)\Delta t) \quad (50)$$

$$t \in [j\Delta t, (j+1)i\Delta t), \quad j = 0, 1, 2, \dots$$

The two kinds of discretization can be carried out with the same approximation number n (number of time steps) since the delay and the time period are the same. While the time-periodicity of the time delay seems to be a further complication, it makes the approximate system simpler since it refers back to the same past value within one time step. This way, the time-periodic delay-differential equation provided in Eq. (47) can be approximated by the linear non-homogeneous ordinary differential equation:

$$\ddot{x}(t) + 2\zeta\omega_n \dot{x}(t) + \omega_n^2 \left(1 + \frac{aK_t}{k_x} A(j\Delta t)\right) x(t) = \omega_n^2 \left(\frac{aK_t}{k_x} A(j\Delta t)\right) x((j-n)\Delta t) \quad (51)$$

for each time interval $t \in [j\Delta t, (j+1)i\Delta t), \quad j = 0, 1, 2, \dots$. Although the average time delay in the approximate system is somewhat larger than the exact delay T , the approximation is convergent by decreasing the size of the time step Δt , that is, by increasing the approximation number n (see [48] for details). Since the right hand side is piece-wise constant, the closed form solution of this approximate system can be obtained similarly to Eq.(30) for the case of highly interrupted cutting. This time, the discrete map expressed in Eq.(33) will have a much larger size. While the piece-wise constant approximation of the periodic function $A(t)$ does not increase the size of this matrix, the intermittent delayed state values do, since not just $x(t)$ and $x(t-T)$, but all the discrete states $x((j-i)\Delta t), \quad (i=0, 1, \dots, n)$ and their time derivatives have to be used as state variables at the j^{th} time instant $t_j = j\Delta t, \quad j = 0, 1, 2, \dots$. This way, the size of the quotient matrix will be at least $2(n+1) \times 2(n+1)$, and its eigenvalues must be checked with appropriate numerical method to have absolute values less than 1.

A typical stability chart is presented in Figure 11, where the effect of the time periodicity is not as strong as in the case of highly interrupted cutting because the milling process with higher number of teeth ($N = 4$), while the radial immersion is still far from full immersion. In this case, the presence of the period-doubling instabilities is not so characteristic and is less relevant. Moreover, as it was proven by Szalai and Stepan [49], these are not lobes anymore, but rather unstable islands (or unstable pockets/lenses), which are mostly surrounded by the classical chatter instability lobes. These unstable islands can still be separated and shifted to the stable domains as fully isolated islands as shown experimentally by Zatarain *et al.*[50], which discusses also further complications when modeling helical cutting edge tools.

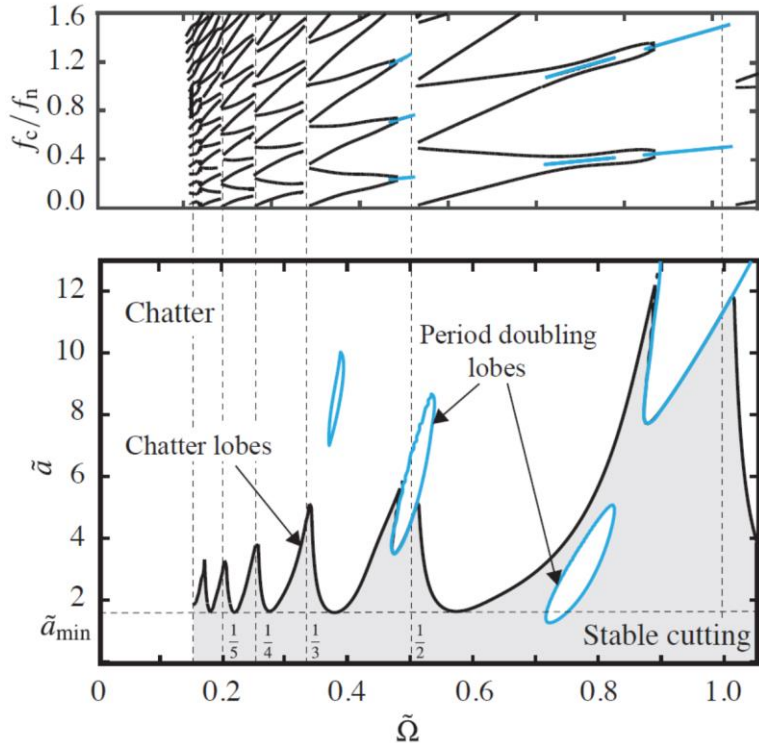


Figure 11 Stability chart of the milling process. The period-doubling lobes become unstable islands. Feed per tooth is 0.1 mm, radial immersion is 0.02, a number of cutting edges is $N=4$, the cutting coefficients are $K_t = 1000$ MPa and $K_r = 0.3$, the damping ratio is $\zeta = 0.05$.

3.3 Milling bifurcations

As described in Sections 3.1-3.3, in the surface regeneration process during milling, a time delay appears in the system of second-order differential equations of motion that describe the dynamic behavior. Specifically, the instantaneous chip thickness, which scales the cutting force, depends not only on the commanded value and current relative vibration between the workpiece and endmill tooth creating the new surface but also on the relative vibration one tooth period earlier (i.e., the surface left by the previous tooth). Due to this time delay, various bifurcations (i.e., the appearance of a qualitatively different solution as a control parameter is varied) are exhibited. These bifurcations include: 1) secondary Hopf instability (classic chatter) which depends on the averaged directional factors; and 2) period-n motions which consider the time-periodic directional factors which have high harmonics at severely intermittent cutting operations.

Drawing from techniques in nonlinear dynamics, analysis tools have been implemented to study bifurcations in milling [51]. These include the phase-space Poincaré map, where the dynamic trajectory of the tool (or workpiece) is presented graphically as the displacement versus velocity and then sampled at the forcing frequency, or tooth period for milling. The character of the once-per-tooth period samples then describes milling behavior. For stable cuts (forced vibration), the motion is periodic with the tooth period, so the sampled points repeat and a single grouping of points is observed. When secondary Hopf instability occurs, the motion is quasi-periodic with tool rotation because the chatter frequency is (generally) incommensurate with the tooth passing frequency. In this case, the once-per-tooth sampled points do not repeat and they form an elliptical distribution. For a period-2 bifurcation (or period-doubling chatter with added lobes as described in Sections 3.2 and 3.3), the motion repeats only once every other cycle (i.e., it is a sub-harmonic

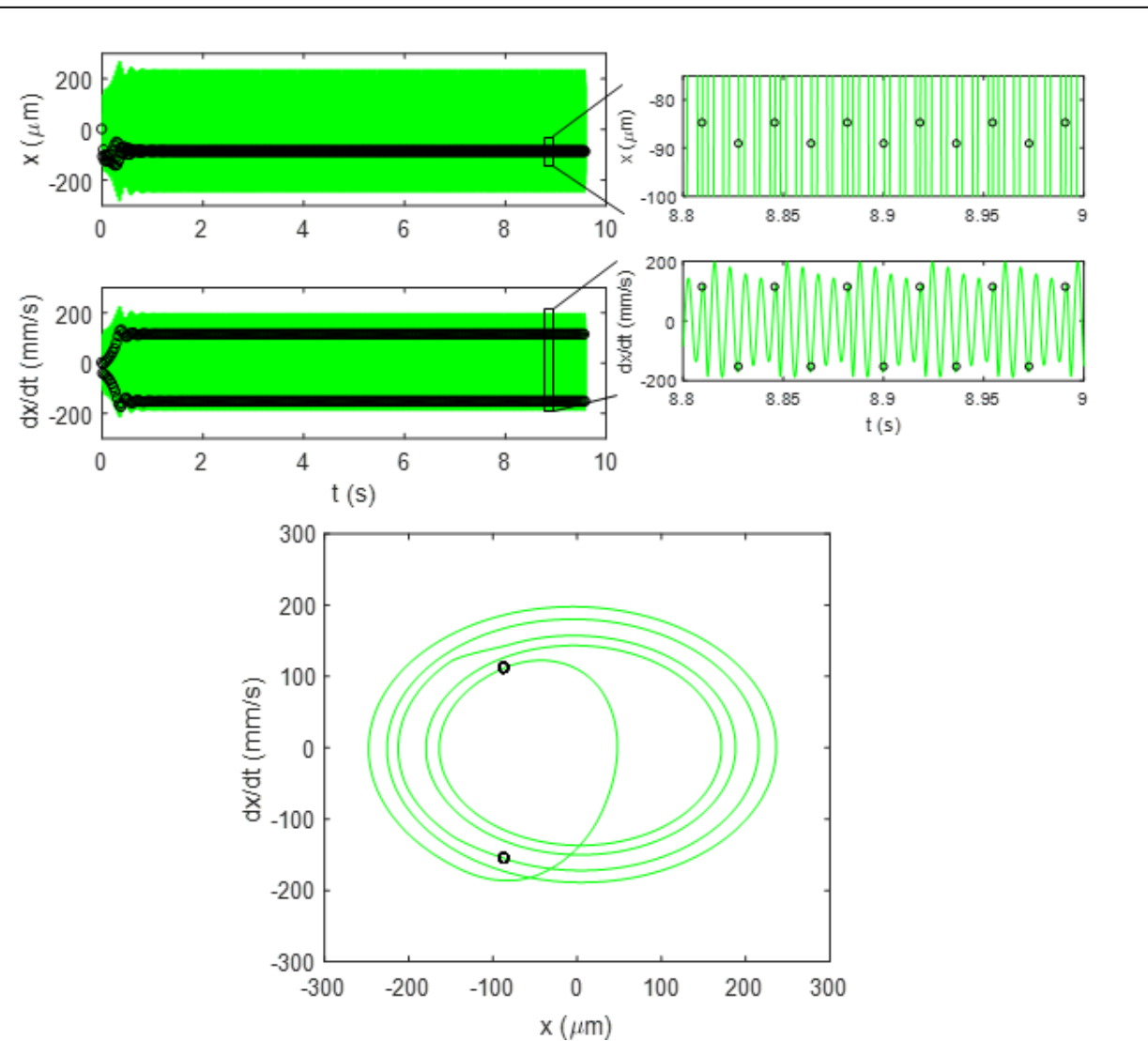


Figure 12 Top) Time domain results for a period-2 bifurcation, i.e. chatter with added lobes. (Bottom) Poincaré map for period-2 bifurcation. The sampled points align at a two fixed locations for the period-2 bifurcation.

of the forcing frequency). In this case, the once-per-tooth sampled points alternate between two solutions. For period-n bifurcations, the sampled points appear at n distinct locations in the Poincaré map.

An example period-2 bifurcation, the chatter with added lobes, is depicted in Figure 12. In the top panel, the time domain displacement and velocity are shown individually. The inset provides a magnified view; it is observed that the sampled points repeat every other tooth period, rather than every period. The bottom panel shows the Poincaré map, where the sampled points appear at two distinct locations.

A second analysis tool is the bifurcation diagram. Here, the independent variable, such as axial depth of cut, is plotted on the horizontal axis against the once-per-tooth sampled displacement on the vertical axis. The transition in stability behavior from stable (at low axial depths) to period-n or secondary Hopf instability (at higher axial depths) is then directly observed. This diagram represents the information from multiple Poincaré maps over a range of, for example, axial depths, all at a single spindle speed. A stable cut appears as a single point (i.e., the sampled points repeat when only forced vibration is present). A period-2 bifurcation, on the other hand, appears as a pair of points offset from each other in the vertical direction. This represents the two collections of once-per-tooth sampled points from the Poincaré map. A secondary Hopf bifurcation is seen as vertical distribution of points; this represents the range of once-per-tooth sampled displacements from the elliptical distribution of points in the Poincaré map.

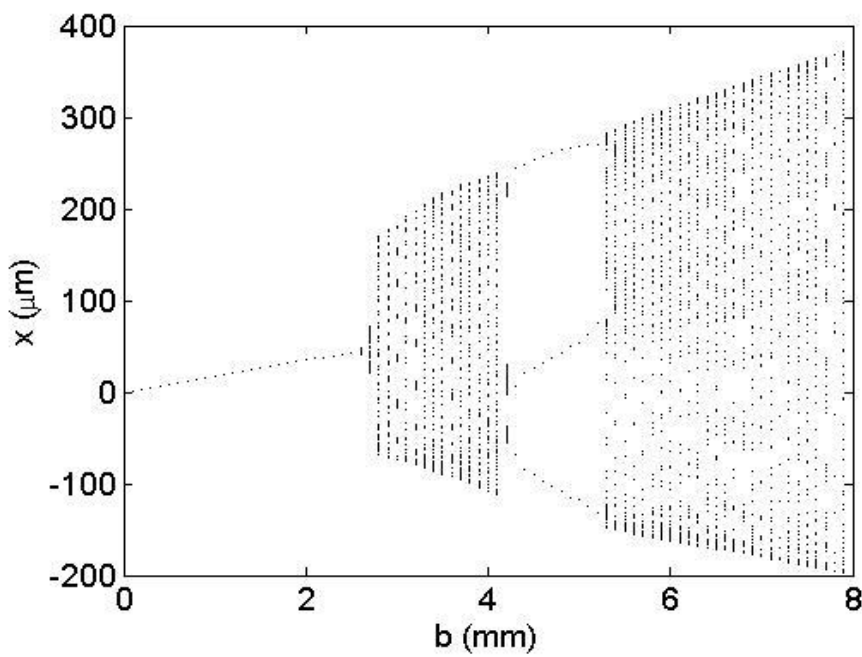


Figure 13 Example bifurcation diagram. Stable behavior is observed up to an axial depth (b) of approximately 2.5 mm. It is indicated by the single value of the sampled feed direction (x) tool displacements. Between 2.5 mm and 4 mm, secondary Hopf chatter with added lobes occurs (i.e., a distribution of sampled points). Between 4 mm and 5.5 mm, a period-3 bifurcation is seen (i.e., three distinct sampled points).

An example bifurcation diagram is provided in Figure 13 [52]. The selected axial depth is listed on the horizontal axis, while the once-per-tooth sampled points for the tool displacement are presented on the vertical axis. All results are for a single spindle speed. It is demonstrated that changing the system gain (axial depth) for a fixed time delay (spindle speed) can transition the behavior from forced vibration (up to 2.5 mm) to secondary Hopf bifurcation chatter with added lobes (between 2.5 mm and 4 mm) to period-3 bifurcation (between 4 mm and 5.5 mm).

In the literature, Davies *et al.* used once per revolution sampling to characterize the synchronicity of cutting tool motions with the tool rotation and first measured period-3 tool motion (i.e., motion that repeated with a period of three cutter revolutions) during partial radial immersion milling [53]. They followed with an analytical map that predicted a doubling of the number of optimally stable spindle speeds when the time in cut is small.

As noted in Sections 3.1-3.3, follow-on modeling efforts included time finite element analysis [44, 45], semi-discretization [54, 55], and the multi-frequency method [22, 23, 42], which were used to produce milling stability charts that predicted both stable and bifurcation behavior. Time marching simulation has also been implemented to study milling bifurcations [56-58]. To aid in the analysis of the simulation results, a new metric was described that automatically differentiates between stable and unstable behavior of different types for time-domain simulation of the milling processes [59, 60]. The approach was based on periodic sampling of milling signals at once per tooth period (harmonic sampling) and integer multiples of the tooth period (subharmonic sampling). The geometric accuracy of parts machined under both stable and period-2 bifurcations was also predicted by time-domain simulation and verified experimentally [61].

3.4 Chatter stability of multi-point tools with lateral, torsional, and axial flexibilities

Any flexible direction that affects the regenerative chip thickness must be considered in the equation of motion with time delay. For example, twist drills have lateral (x, y) and torsional (θ) flexibilities that create the axial (z) vibrations which change the regenerative chip thickness as shown in Figure 14. The dynamics of a twist drill with such flexibilities may be expressed as:

$$\mathbf{M}\ddot{\mathbf{q}}(t) + \mathbf{C}\dot{\mathbf{q}}(t) + \mathbf{K}\mathbf{q}(t) = \mathbf{F}(\mathbf{q}(t), \mathbf{q}(t-T)), \quad (52)$$

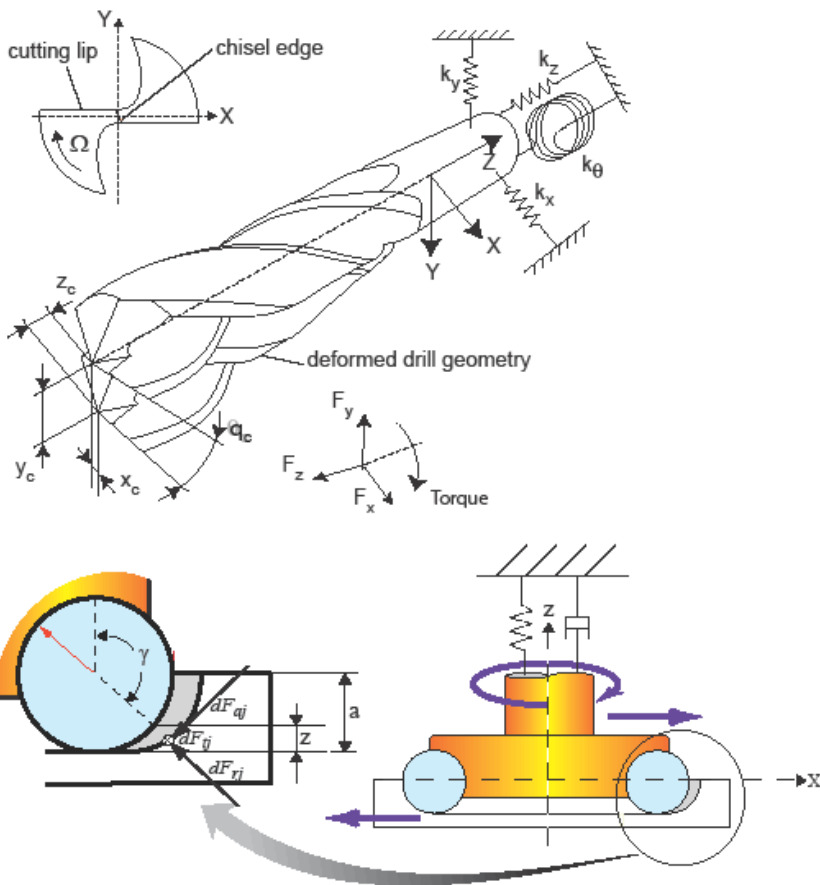


Figure 14 Dynamic flexibilities of a twist drill and milling cutter with circular inserts.

where the vibration vector $\mathbf{q}(t) = \{x(t) \quad y(t) \quad z(t) \quad \theta(t)\}$ has lateral (x, y), axial (z), and torsional (θ) vibrations. The force vector is $\mathbf{F}(t) = \{\mathbf{F}_x(t) \quad \mathbf{F}_y(t) \quad \mathbf{F}_z(t) \quad \mathbf{T}_c(t)\}$ where (\mathbf{T}_c) is the cutting torque. The FRF in Eq. (44) becomes [62]:

$$\Phi(\omega) = \begin{bmatrix} \Phi_{xx} & \Phi_{xy} & 0 & 0 \\ \Phi_{yx} & \Phi_{yy} & 0 & 0 \\ 0 & 0 & \Phi_{zz} & \Phi_{z\theta} \\ 0 & 0 & \Phi_{\theta z} & \Phi_{\theta\theta} \end{bmatrix}, \quad (53)$$

where $\Phi_{\theta\theta}$ is the torsional FRF excited by the drilling torque and $\Phi_{z\theta}$ is the FRF contributed by the torsional-axial coupling of vibrations. The eigenvalue problem becomes four-dimensional in Eq. (44), but the frequency and semi-discrete time-domain solution methods remain the same. Boring heads and plunge mills have the same dynamics as twist drills [63]. The same argument is valid for workpieces where there may be cross-coupling of the structure in different directions. Milling

tools with ball ends or circular inserts also have the same stability model but present two and three-dimensional eigenvalue problems since regeneration may take place both in the lateral and axial directions due to its flexibility [64-66], but no torsional-axial coupling is considered. The lead and tilt angles of the tools in five-axis ball-end milling of curved surfaces can be optimized to increase the stability [67, 68].

4. Suppression of chatter with non-uniform tools

The chatter stability limit can be increased using tool holders with tuned damper mechanisms [69, 70], active damping using actuators [17], or special tool geometries which create stability pockets at the desired speeds by proper selection of the tooth spacing angles, variable helix, or serrated cutting edges. Only the tool design methods are summarized here.

The main principle behind the variable pitch, or unequally spaced, teeth on milling tools is to alter the delay which is responsible for the regeneration mechanism. The effectiveness of variable pitch cutters in suppressing chatter vibrations in milling was first demonstrated by Slavicek [71]. He assumed a rectilinear tool motion for the cutting teeth and applied the orthogonal stability theories of Tlusty and Tobias for the irregular tooth pitch case. By assuming an alternating pitch variation, he obtained an expression for the stability limit which was a function of the pitch variation. Successive cutting teeth were separated by a distance l_j which was different for each interval as shown in Figure 15.

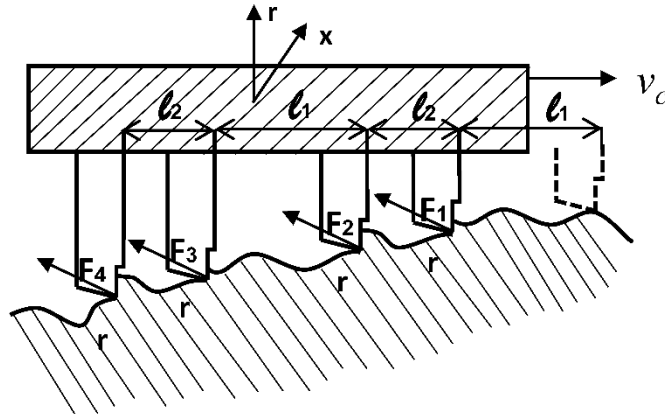


Figure 15 Rectilinear representation of variable pitch milling tool proposed by Slavicek [71].

Slavicek [71] expressed the dynamic forces on N cutting teeth as:

$$F_j = -K_t a \left(r - r e^{-i\varphi_j} \right) \text{ for } j = 1, N, \quad (54)$$

where F_j is the dynamic cutting force on tooth j , r is the vibration amplitude, and φ_j is the phase shift or delay between the waves, i.e., the inner and outer modulations. The phase shift is different for each cutting tooth due to the unequal distance between each successive tooth:

$$\varphi_j = \frac{\omega_c l_j}{v_c}, \quad (55)$$

where ω_c is the chatter frequency and v_c is the cutting speed. This simple relation shows that the tooth spacing and the cutting speed affect the delay, hence the tooth spacing l_j can be selected to minimize the delay φ_j to increase the stability.

Opitz *et al.* [72] considered milling tool rotation using average directional factors in analyzing stability with irregular tooth pitch. They also considered alternating pitch with only two different pitch angles. Average directional factors which relate the dynamic chip thickness to the vibrations do not accurately represent the tool rotation which causes time-varying milling dynamics. A comprehensive study on the stability of milling tools with non-constant pitch was carried out by Vanherck [73] using computer simulations. His study demonstrated that a certain pitch variation pattern was effective, i.e., increased the stability limits significantly for a given milling system over a certain cutting speed range. This fundamental idea was later used in several works for optimal design of variable pitch tools.

Thusty *et al.* [74] presented the stability of milling cutters with special geometries such as irregular pitch or serrated edges using numerical simulations. Their numerical simulations showed the effectiveness of irregular milling tool geometries and cutting edges in increasing stability against chatter. Later, Altintas *et al.* [75] analyzed the stability of variable pitch cutters accurately using their analytical milling stability model [24]. The analytical model considers tool rotation, time-varying dynamics, and multiple vibration modes, hence their experimentally verified predictions were more accurate. They considered both linear and alternating pitch variations and showed that each variation pattern had an effective zone where chatter stability limits were increased substantially compared to standard milling tools. Olgac *et al.* used the same dynamic model of variable pitch milling operations, but proposed a parametric stability analysis [76]. These studies mainly concentrated on the effect of pitch variation on the stability limit; they did not directly address the cutting tool design to determine the optimal pitch variation, although they can be used to see the effectiveness of various tool designs. Budak [77] proposed an optimization methodology for the design of variable pitch tools considering the chatter frequency and spindle speed. The spacing variation amount is related to the chatter waves left on the surface in order to establish the linear pitch angle variation as $\phi_p, \phi_p + \Delta\phi, \phi_p + 2\Delta\phi, \dots$ where ϕ_p is the base pitch angle and $\Delta\phi$ is the pitch angle increment between the successive teeth. Budak [76] showed that the eigenvalue solution in the analytical chatter stability model takes the following form for variable pitch tools:

$$\Lambda = \frac{a}{4\pi} K_t \sum_{j=1}^N \left(1 - e^{-i\omega_c T_j} \right), \quad (56)$$

where T_j is the tooth period which is variable due to non-constant pitch angles and a is the depth of cut. Budak obtained the following simple equation for the critically stable depth of cut in the case of variable pitch milling tools:

$$a_{\lim}^{vp} = -\frac{4\pi}{K_t} \frac{\Lambda_I}{S} \quad (57)$$

where Λ_I is the imaginary part of the eigenvalue and

$$S = \sum_{j=1}^N \sin \omega_c T_j \quad \text{or} \quad S = \sin \varepsilon_1 + \sin \varepsilon_2 + \sin \varepsilon_3 + \dots$$

represents the summation of the phase delays caused by each tooth interval. This equation implied that S must be minimized to maximize the chatter stability limit using variable pitch end mills. The effect of the phase variation due to the variable pitch tool on the stability gain, which is defined as the stability limit for the variable pitch tool over the one with the standard tool, was investigated and it was shown that for particular values of the delay $\Delta\varepsilon$, the stability limit was maximized as illustrated in Figure 16.

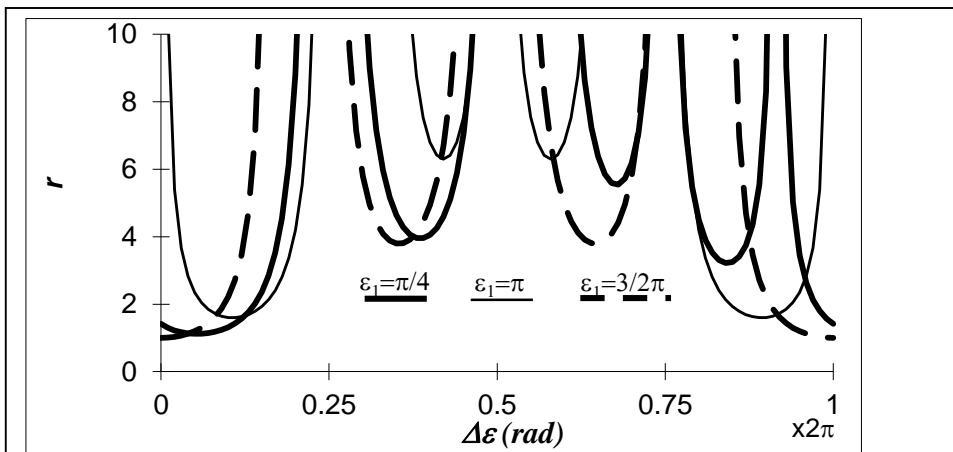


Figure 16 Effect of $\Delta\varepsilon$ on stability gain for a four-tooth end mill with linear pitch variation.

Budak [77] showed that this condition could be achieved if the variation amount was selected as follows:

$$\begin{aligned} \Delta\varphi &= \pi \frac{\Omega}{\omega_c} && \text{for even } N \\ \Delta\varphi &= \pi \frac{\Omega}{\omega_c} \frac{(N \pm 1)}{N} && \text{for odd } N \end{aligned} \quad (58)$$

where Ω is the spindle speed in (rad/sec), $\Delta\varphi$ is the pitch variation (rad), ω_c is the chatter frequency (rad/sec), and N is the number of teeth. Note that the additional phase delay introduced by the optimal pitch variation is set as integer divisions of the original delay of the milling system in a standard tool. The pitch variation should cancel the “remainder wave” for maximized stability.

It can be seen from Eq. (58) that the required pitch variation is proportional to the spindle speed. As discussed in [78], large pitch variations required for high speeds cause non-uniform chip loads on the cutting edges whereas small pitch variations in the low speed zone become sensitive to slight changes in the chatter frequency. The formulation neglected the effect of pitch variation on the chatter frequency by using a variable pitch tool; the chatter frequency was obtained experimentally using a standard end mill. This issue was addressed by Comak *et al.* [79] where the predicted effect of pitch variation on the chatter frequency was considered when selecting the optimal pitch angles as shown in Figure 17. As this figure illustrates, the effect of the pitch angle variation on the chatter frequency can be significant and should, therefore, be taken into account in the selection of angles for variable pitch tools. Also, different pitch variations may yield similar increases in the stability limits as shown in Figure 17, which shows that small pitch angle variation can yield significant productivity gain using the proposed optimization approach.

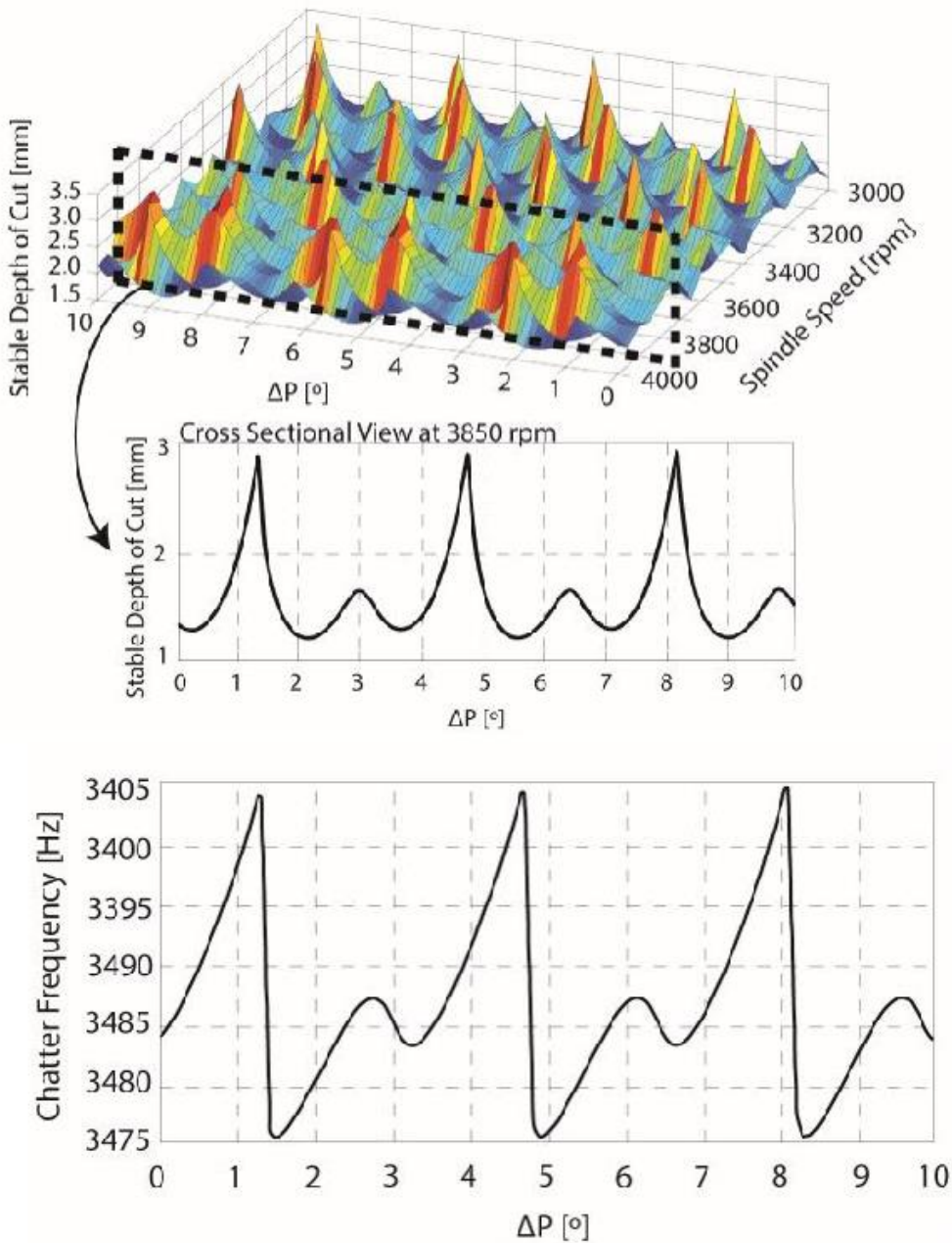


Figure 17. The effect of pitch angle variation on the stable depth of cut for different spindle speeds and on the chatter frequency [77].

Also note that the closer the tooth passing frequency is to the chatter frequency, the larger the pitch variation will be as evident from Eq.(58). As a result, variable pitch cutters become more practical to use at low speeds where the tooth passing frequencies are several times lower than the chatter frequency, such as in machining titanium and nickel alloys used in the aerospace industry.

Alternatively, or in combination with variable pitch tools, end mills with varying helix angles have also been introduced to vary pitch angle along the tool axis [80-82]. Serration on the end mill's cutting edges creates pitch angle variation between the teeth at each elevation, which also disturbs regeneration [83, 84]. A sample comparison of chatter stability lobes with and without serration is presented by Merdol *et al.* [83] as shown in Figure 18. Tehranizadeh *et al.* [85] optimized the shapes of serrat waves to reduce the cutting forces. Their results show that optimized tools have better chatter stability performance due to the reduction of the effective axial depth of cut which is possible at lower feed rates.

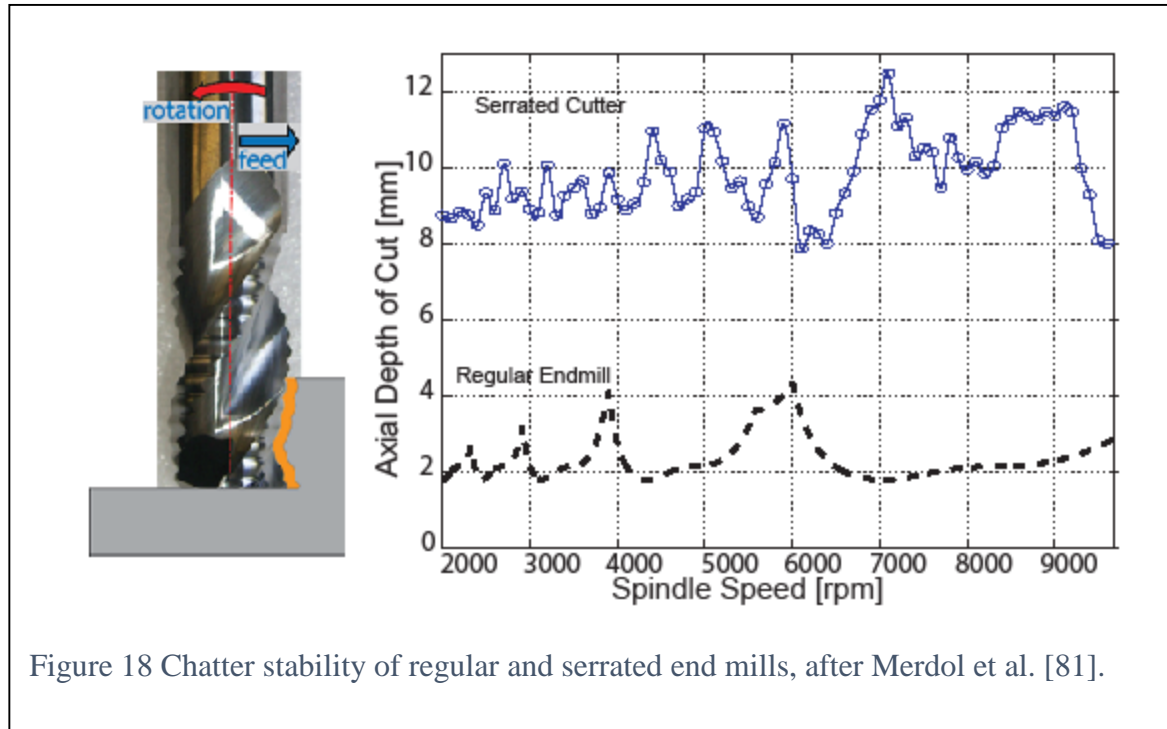


Figure 18 Chatter stability of regular and serrated end mills, after Merdol et al. [81].

5. Stability of parallel machining operations

Parallel, or simultaneous, machining has received considerable attention in the industry due to its potential to increase the material removal rate (MRR). However, parallel machining can be susceptible to chatter due to the dynamic interaction between the system components unless stable process parameters are selected. The parallel turning and milling operations shown in Figure 19 are presented here as examples.

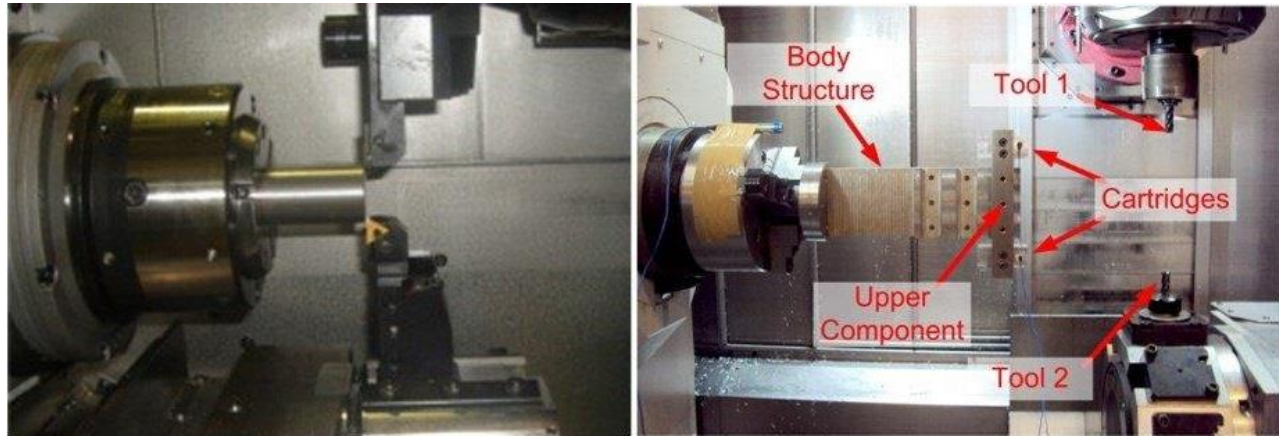


Figure 19 (a) Parallel turning[85] and (b) parallel milling operations [92].

5.1 Parallel turning

In parallel turning, the cutting tools may dynamically interact through: (a) the shared cutting surface, (b) the tool holder structure, and (c) the workpiece structure. Lazoglu *et al.* [86] developed a time-domain model for chatter and stability of parallel turning where the tools cut different surfaces and interact with each other due to the flexibility of the workpiece structure. A one-dimensional frequency domain analysis of chatter in parallel turning operations was presented by Budak *et al.* [87] where tools were mounted on different turrets and cut a shared surface with different depth of cuts as shown in Figure 19a. The dynamic cutting forces have multiple time delays:

$$\begin{Bmatrix} F_1(t) \\ F_2(t) \end{Bmatrix} = K_r \begin{Bmatrix} a_1 \left(-z_1(t) + z_2 \left(t - \frac{\tau}{2} \right) \right) \\ a_1 \left(-z_2(t) + z_1 \left(t - \frac{\tau}{2} \right) \right) + (a_2 - a_1)(-z_2(t) + z_2(t - \tau)) \end{Bmatrix}, \quad (59)$$

where K_r is the cutting force coefficient in the feed direction, z_1 and z_2 are the displacements of the first and second tool in the feed direction, respectively; and τ is the workpiece rotation period. The depth of cuts for the first and second tools are represented by a_1 and a_2 , ($a_2 > a_1$), respectively (Figure 20a). In this model, two regions on the shared surface can exist since the tools' depths of cut can be different. In the first region, both tools remove the same depth of cut a_1 . Therefore, the displacement of each tool at any instant is influenced by the other tool's displacement at the half rotation period of the workpiece before. However, in the second region, the depth ($a_2 - a_1$) is removed by the second tool solely. Thus, the displacement of the second tool at time t is affected by its displacement at the previous rotation period of the workpiece. The eigenvalue problem for the marginally-stable case is formulated in the frequency domain and solved numerically. The solution is provided for the first tool's depth of cut over a range of spindle speed values while the

second tool's depth of cut is initially selected. Figure 20b shows the stability lobe diagram for the first tool where $a_2 = 1.5$ mm. In this case, when $a_1 = 0$ mm (point d) chatter occurs. By increasing a_1 to 1 mm (point e), the productivity is increased and the process is stabilized. By further increasing the a_1 value to 1.5 mm (point f), chatter again occurs. Simulation results were validated with cutting tests in [87].

Ozturk *et al.* [88] presented the chatter stability model for parallel turning operation with two different tool configurations. In the first configuration, the tools were mounted on a turret. In this case, the dynamic displacements of the tools do not interact via the shared surface but rather by the turrets. The results showed that by employing the second tool, the stability limit of the first tool slightly decreases compared to single tool turning. However, the overall material removal rate of the parallel process is almost doubled due to having a second tool. For the second configuration, cutting a shared surface (similar to [87]), they showed that tools with identical natural frequencies have the lowest stability limit. Similar behavior was reported by Reith *et al.* [89] who included the effect of the tool holder using a non-proportional damping model. Brecher *et al.* [90] studied the effect of the radial orientation of the tools when they cut a shared surface with identical depths of cut (see Figure 20b). It was demonstrated that by properly setting the tool's orientation, the stability boundaries can be shifted upwards. For highly flexible workpieces, it is essential to model the true geometry of the insert due to the dominance of the cutting forces in the radial direction as demonstrated by Azvar *et al.* [91]. They concluded that when cutting a shared surface of a flexible workpiece, tools with identical insert geometry demonstrate a higher stability limit. Also, for the case of the parallel turning of a flexible workpiece from different surfaces, the tool which is closer to the free end of the workpiece should have a smaller nose radius and side edge cutting angle to obtain higher stability.

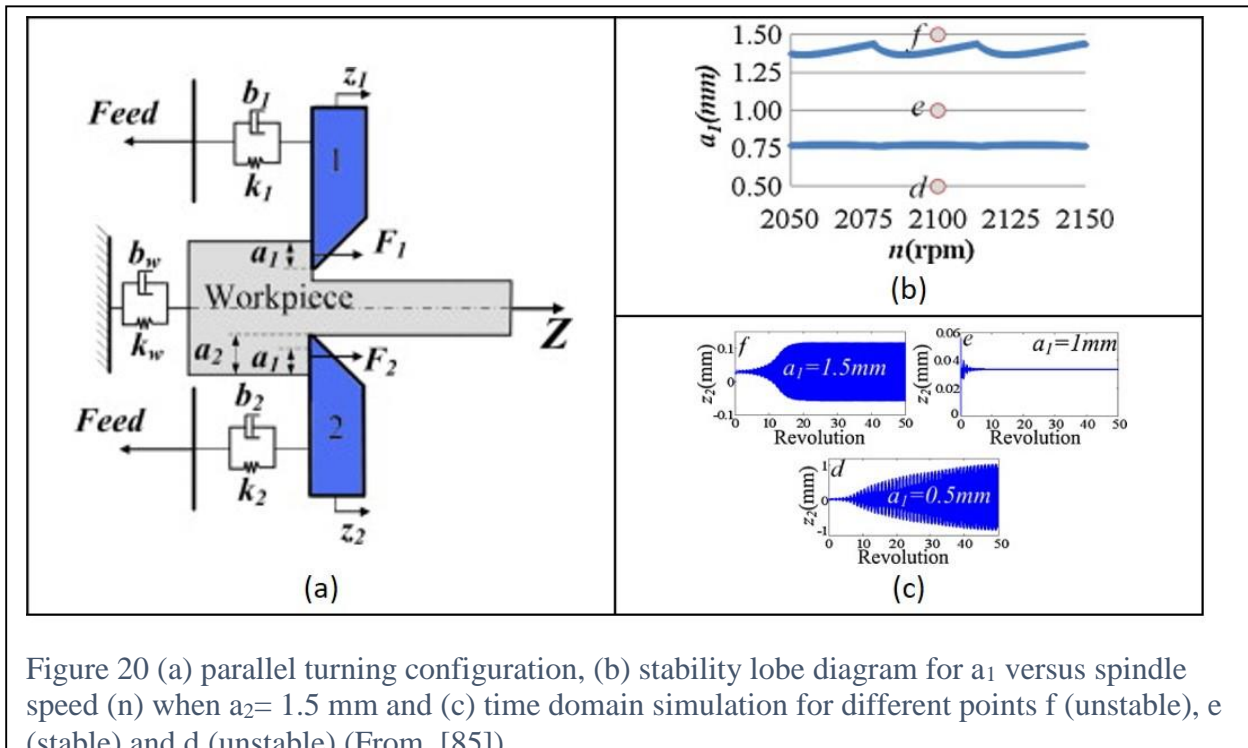


Figure 20 (a) parallel turning configuration, (b) stability lobe diagram for a_1 versus spindle speed (n) when $a_2 = 1.5$ mm and (c) time domain simulation for different points f (unstable), e (stable) and d (unstable). (From [85])

5.2 Parallel milling

Two milling tools cut the workpiece simultaneously in parallel milling operations where the stability limit can be increased due to the cancellation of the dynamic cutting forces. Shamoto *et al.* [92] introduced a technique to eliminate the chatter vibrations in simultaneous face milling of flexible parts by imposing a phase shift resulting from different rotational speeds of milling tools. Budak *et al.* [93] developed the frequency domain stability model for parallel milling systems. The dynamic forces are evaluated analytically to form the characteristic force function:

$$\begin{Bmatrix} F_{x1} \\ F_{y1} \\ F_{x2} \\ F_{y2} \end{Bmatrix} e^{i\omega_c t} = \frac{1}{4\pi} [\text{CPM}] \cdot [\text{DM}] \cdot [\text{OTF}] \cdot \begin{Bmatrix} F_{x1} \\ F_{y1} \\ F_{x2} \\ F_{y2} \end{Bmatrix} e^{i\omega_c t}, \quad (60)$$

where [CPM] is the cutting parameters matrix, [DM] is the delay matrix which includes the phase delays for the milling tools, and [OTF] is the oriented transfer function matrix. Equation (60) results in an eigenvalue problem that provides the experimentally proven stable depths for different spindle speeds; see Figure 21.

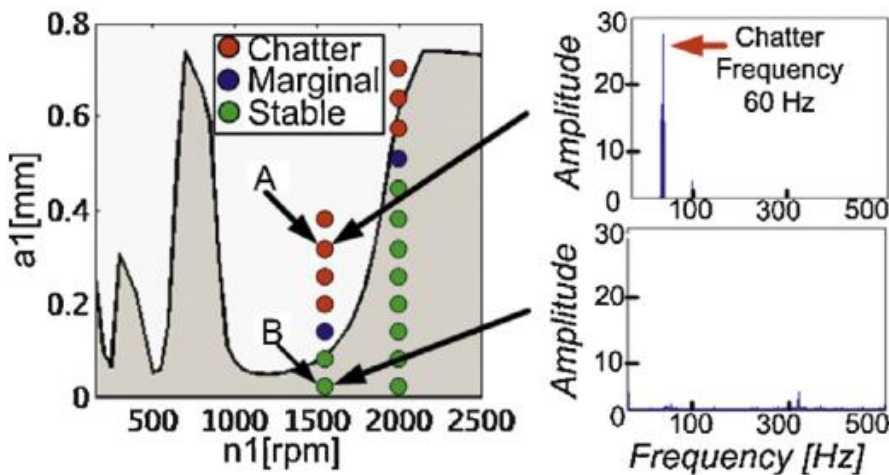


Figure 21 Predicted stability lobe diagram and the experimental results.

6. Current Challenges in machining dynamics

Chatter is still the main obstacle to achieve precision and productivity for machining and grinding operations. Chatter can also be found in other operations, such as rolling [94] and sawing [95] operations. The prediction of chatter-free cutting conditions primarily depends on the identification of machine's structural dynamics, cutting force and process damping coefficients,

and tool-workpiece engagement conditions. Each subject has its own nonlinearities and uncertainties.

The structural dynamics (FRF) as reflected at the tool point (i.e., the tool point receptance) is highly critical in predicting the stability charts. While modal analysis may be applied to measure receptances, this can pose a significant obstacle when equipment or expertise is not available in the production facility. Schmitz and Donaldson first presented the receptance coupling substructure analysis (RCSA) approach to predict tool point receptances by joining models and measurements of the tool, holder, spindle, and machine through appropriate connection parameters [96]. Follow on work by Schmitz *et al.* includes a three-component model [97], at-speed predictions [98], and improved spindle receptance identification [98]. Others have considered the flute geometry [99], the asymmetric dynamics of rotating tools [100], and the elastic coupling of tool and holders with the spindle [101]. Furthermore, the FRF of the machine may change as a function of speed [102], cutting loads, and the position of the machine during machining [103, 104]. Additionally, machining with robots or machines with parallel kinematic configurations have pose-dependent dynamics; therefore, their stability varies along the tool path [105, 106]. As the material is removed during machining, parts with thin-walled structures have continuously varying dynamics which need to be updated along the tool path [107]. Another challenge is the use of multiple spindles to cut a single part simultaneously as presented in Section 5. While one spindle may mill the part, another spindle may carry out grinding, turning, or drilling operation on the same part when using multi-functional machine tools [108]. The cross-talk between the spindles and multiple delays introduce challenges when modeling the process dynamics and its stability, such as in the case of mill-turn operations [109]. There are some heavy duty machining applications at low speeds that excite the low frequency modes of the large components of the machine tools. These low frequency modes shift as the position of the machine vary. Iglesias *et al.* [110] proposed position and feed direction dependent stability charts in planning heavy duty cutting of steel alloys within the operating envelope of large machine tools.

Cutting tools have rounded and chamfered cutting edges that are not consistently manufactured. The force required to shear away the chip is split into the ploughing and cutting components, depending on the relative sizes of the cutting edge radius and the chip [111]. Furthermore, the wear changes the contact between the wavy cut surface and the tool's flank face that contributes to the process damping [32]. As a result, the cutting force and process damping coefficients have significant uncertainties. Since the cutting force coefficient acts as a gain and the process damping coefficient improves the stability, uncertainties in these parameters affects the accuracy of chatter predictions. For example, the process damping is challenging to model in twist drills where the cutting speed starts from zero at the chisel tip and increases towards the periphery [112].

When the cutter shape is irregular as in form tools, serrated end mills, and multi-functional tools which may include drilling, boring, and chamfering in a single operation, the cutter-part engagement conditions may change along the tool axis [113, 114]. As a result, the directional coefficient matrix, as well as the process dynamics, may vary significantly as in the case of threading [115] and gear machining with multiple teeth [116]. Efficient modeling and the stability solution for such tools and operations are still needed for high-performance machining. A recent

metrology solution is structured light scanning, which can be used to measure the actual cutting edge geometry [117].

7. Conclusion

This paper presents the fundamentals of chatter stability laws developed in the frequency and discrete-time domains. It is shown that the dynamics of the machining process need to be modeled by considering the interaction between the machining process and the structural dynamics of both the machine and the machined part. The dynamics can be stationary with time-invariant coefficients, such as in turning, or time-periodic with time-varying delays as in the case of turn-milling operations. Although the understanding of stability for dynamic machining has increased significantly during last six decades, the accuracy of stability predictions still suffers due to measurement uncertainties, nonlinearities in the machine structure and process, time-varying dynamics of machine tools and parts, and ploughing-based material removal by a worn tool or chamfered cutting edge. The integration of physics-based off-line chatter prediction models needs to be combined with on-line, adaptive learning and tuning techniques for robust chatter detection and avoidance. Complex processes such as gear shaping with form tools, the stability of machining composite metals, and additively manufactured parts with non-uniform material properties remain to be studied.

Acknowledgments: The authors acknowledge the Natural Sciences and Engineering Council of Canada Grants (IRCPJ 260683-18 and CANRIMT NETGP 479639-15); USA National Science Foundation Grant (CMMI-1561221); TUBITAK-Turkey Grant Numbers: 105M032, 108M340, 110M522, 217M210; Hungarian National Research, Development and Innovation Fund (TUDFO/51757/2019-ITM Thematic Excellence Program; and the Research Excellence Program under Grant no. KKP133846.

References

- [1] Taylor, F. W., 1906, "On the art of cutting metals," Transactions, The American Society of Mechanical Engineers, 28, pp. 70-350.
- [2] Arnold, R. N., 1946, "Cutting tools research: report of subcommittee on carbide tools: the mechanism of tool vibration in the cutting of steel," P I Mech Eng B-J Eng, 154/1, pp. 261-284.
- [3] Doi, S., and Kato, S., 1956, "Chatter vibration of lathe tools," Trans. ASME 78, p. 1127.
- [4] Tobias, S., and Fishwick, W., 1958, "Theory of regenerative machine tool chatter," The engineer, 205/7, pp. 199-203.
- [5] Tlusty, J., and Polacek, M., 1963, "The stability of the machine tool against self excited vibration in machining.," Proceedings of the ASME International Research in Production Engineering.Pittsburgh, pp. 465-474.
- [6] Tlusty, J., 1978, "Analysis of the state of research in cutting dynamics," Annals of the CIRP, 27/2, pp. 583-589.
- [7] Tlusty, J., 1986, "Dynamics of High-Speed Milling," ASME Journal of Engineering for Industry, 108(2), pp. 59-67.
- [8] Altintas, Y., and Weck, M., 2004, "Chatter stability of metal cutting and grinding," Cirp Annals-Manufacturing Technology, 53(2), pp. 619-642.
- [9] Wiercigroch, M., and Budak, E., 2001, "Sources of nonlinearities, chatter generation and suppression in metal cutting," Philos T R Soc A, 359(1781), pp. 663-693.

- [10] Quintana, G., and Ciurana, J., 2011, "Chatter in machining processes: A review," International Journal of Machine Tools and Manufacture, 51/5, pp. 363-376.
- [11] Altintas, Y., Stepan, G., Merdol, D., and Dombovari, Z., 2008, "Chatter stability of milling in frequency and discrete time domain," CIRP Journal of Manufacturing Science and Technology, 1/1, pp. 35-44.
- [12] Merritt, H. E., 1965, "Theory of Self-Excited Machine-Tool Chatter: Contribution to Machine-Tool Chatter Research—," Journal of Engineering for Industry, 87/4, pp. 447-454.
- [13] Koenigsberger, F., and Tlusty, J., 1970, Structures of machine tools, Pergamon Press, Oxford.
- [14] Smith, S., and Tlusty, J., 1997, "Current trends in high-speed machining," ASME Journal of Manufacturing Science and Engineering, 119(4B), pp. 664-666.
- [15] Abele, E., Altintas, Y., and Brecher, C., 2010, "Machine tool spindle units," Cirp Annals-Manufacturing Technology, 59/2, pp. 781-802.
- [16] Sweeney, G., and Tobias, S., 1969, "Survey of basic machine tool chatter research," International Journal of Machine Tool Design, 9/3, pp. 217-238.
- [17] Munoa, J., Beudaert, X., Dombovari, Z., Altintas, Y., Budak, E., Brecher, C., and Stepan, G., 2016, "Chatter suppression techniques in metal cutting," Cirp Annals-Manufacturing Technology, 65(2), pp. 785-808.
- [18] Tunc, L. T., Mohammadi, Y., and Budak, E., 2018, "Destabilizing effect of low frequency modes on process damped stability of multi-mode milling systems," Mechanical Systems and Signal Processing, 111, pp. 423-441.
- [19] Sridhar, R., Hohn, R. E., and Long, G. W., 1968, "A Stability Algorithm for the General Milling Process: Contribution to Machine Tool Chatter Research," ASME Journal of Engineering for Industry, 90/2, pp. 330-334.
- [20] Minis, I., Yanushevsky, R., Tembo, A., and Hocken, R., 1990, "Analysis of Linear and Nonlinear Chatter in Milling," CIRP Annals, 39/1, pp. 459-462.
- [21] Minis, I., and Yanushevsky, R., 1993, "A New Theoretical Approach for the Prediction of Machine Tool Chatter in Milling," Journal of Engineering for Industry, 115/1, pp. 1-8.
- [22] Budak, E., and Altintas, Y., 1998, "Analytical prediction of chatter stability in milling - Part 1: General formulation," Transcation of ASME, Journal of Dynamic Systems Measurement and Control, 120/1, pp. 22-30.
- [23] Budak, E., and Altintas, Y., 1998, "Analytical prediction of chatter stability in milling - Part II: Application of the general formulation to common milling systems," Transactions of the ASME, Journal of Dynamic Systems Measurement and Control, 120/1, pp. 31-36.
- [24] Altintas, Y., and Budak, E., 1995, "Analytical Prediction of Stability Lobes in Milling," CIRP Annals, 44/1, pp. 357-362.
- [25] Stépán, G., 1998, "Delay-differential equation models for machine tool chatter," Dynamics and chaos in manufacturing processes, Wiley, New York, pp. 165-192.
- [26] Insperger, T., and Stépán, G., 2000, "Stability of the milling process," Periodica Polytechnica, Mechanical Engineering, 44/1, pp. 47-57.
- [27] Merchant, M. E., 1945, "Mechanics of the metal cutting process. I. Orthogonal cutting and a type 2 chip," Journal of applied physics, 16(5), pp. 267-275.
- [28] Budak, E., Altintas, Y., and Armarego, E. J. A., 1996, "Prediction of milling force coefficients from orthogonal cutting data," Transactions of ASME Journal of Manufacturing Science and Engineering, 118/2, pp. 216-224.

- [29] Ehmann, K., Kapoor, S., DeVor, R., and Lazoglu, I., 1997, "Machining process modeling: a review," ASME Journal of Manufacturing Science, 119(4B), pp. 655-663.
- [30] Ismail, F., and Vadari, V., 1990, "Machining chatter of end mills with unequal modes," ASME Journal of Engineering for Industry, 112(3), pp. 229-235.
- [31] Das, M. K., Tobias, S.A., , 1967, "The relation between the static and the dynamic cutting of metals," International Journal of Machine Tool Design and Research, 7(2), pp. 63-68.
- [32] Eynian, M., and Altintas, Y., 2009, "Chatter Stability of General Turning Operations With Process Damping," Transactions of ASME Journal of Manufacturing Science and Engineering, 131(4), p. 041005.
- [33] Altintas, Y., 2012, Manufacturing Automation: Metal Cutting Mechanics, Machine Tool Vibrations, and CNC Design, Cambridge University Press, Cambridge.
- [34] Tyler, C. T., and Schmitz, T. L., 2013, "Analytical process damping stability prediction," Journal of Manufacturing Processes, 15(1), pp. 69-76.
- [35] Budak, E., and Tunc, L. T., 2010, "Identification and modeling of process damping in turning and milling using a new approach," CIRP Annals, 59(1), pp. 403-408.
- [36] Altintas, Y., Eynian, M., and Onozuka, H., 2008, "Identification of dynamic cutting force coefficients and chatter stability with process damping," Cirp Annals-Manufacturing Technology, 57(1), pp. 371-374.
- [37] Ahmadi, K., and Altintas, Y., 2014, "Identification of Machining Process Damping Using Output-Only Modal Analysis," Journal of Manufacturing Science and Engineering-Transactions of the Asme, 136(5).
- [38] Tuysuz, O., and Altintas, Y., 2019, "Analytical Modeling of Process Damping in Machining," Trans. ASME Journal of Manufacturing Science and Engineering, pp. 1-52.
- [39] Dombovari, Z., Iglesias, A., Zatarain, M., and Insperger, T., 2011, "Prediction of multiple dominant chatter frequencies in milling processes," International Journal of Machine Tools and Manufacture, 51(6), pp. 457-464.
- [40] Davies, M. A., Balachandran, B., 2000, "Impact Dynamics in the Milling of Thin-Walled Structures," Nonlinear Dynamics, 22(4), p. 17.
- [41] Davies, M. A., Pratt, J. R., Dutterer, B., and Burns, T. J., 2002, "Stability Prediction for Low Radial Immersion Milling," Journal of Manufacturing Science and Engineering, 124(2), pp. 217-225.
- [42] Merdol, S. D., and Altintas, Y., 2004, "Multi Frequency Solution of Chatter Stability for Low Immersion Milling," Journal of Manufacturing Science and Engineering, 126(3), pp. 459-466.
- [43] Bayly, P. V., Halley, J. E., Mann, B. P., and Davies, M. A., 2003, "Stability of Interrupted Cutting by Temporal Finite Element Analysis," Journal of Manufacturing Science and Engineering, 125(2), pp. 220-225.
- [44] Insperger, T., Mann, B. P., St  p  n, G., and Bayly, P. V., 2003, "Stability of up-milling and down-milling, part 1: alternative analytical methods," International Journal of Machine Tools and Manufacture, 43(1), pp. 25-34.
- [45] Mann, B. P., Insperger, T., Bayly, P. V., and St  p  n, G., 2003, "Stability of up-milling and down-milling, part 2: experimental verification," International Journal of Machine Tools and Manufacture, 43(1), pp. 35-40.
- [46] Gradi  ek, J., Kalveram, M., Insperger, T., Weinert, K., St  p  n, G., Govekar, E., and Grabec, I., 2005, "On stability prediction for milling," International Journal of Machine Tools and Manufacture, 45(7), pp. 769-781.

- [47] Merdol, D., 2008, "Virtual three-axis milling process simulation and optimization," Ph.D. , University of British Columbia.
- [48] Insperger, T., Stepan, G., 2011, Semi-Discretization for Time-Delay Systems, Springer, New York.
- [49] Szalai, R., Stepan, G., 2006, "Lobes and lenses in the stability chart of interrupted turning. Journal of Computational and Nonlinear Dynamics," Transactions of ASME, Journal of Computational and Nonlinear Dynamics, 1, p. 6.
- [50] Zatarain, M., Muñoa, J., Peigné, G., and Insperger, T., 2006, "Analysis of the Influence of Mill Helix Angle on Chatter Stability," CIRP Annals, 55(1), pp. 365-368.
- [51] Moon FC, K.-N. T., 2001, "Nonlinear models for complex dynamics in cutting materials.," Philosophical Transactions of the Royal Society London A(359), pp. 695-711.
- [52] Honeycutt, A., and Schmitz, T. L., 2018, "Milling Bifurcations: A Review of Literature and Experiment," Journal of Manufacturing Science and Engineering, 140(12), pp. 120801-120801-120819.
- [53] Davies, M. A., Dutterer, B., Pratt, J. R., Schaut, A. J., and Bryan, J. B., 1998, "On the Dynamics of High-Speed Milling with Long, Slender Endmills," CIRP Annals, 47(1), pp. 55-60.
- [54] Insperger, T., and Stépán, G., 2004, "Vibration Frequencies in High-Speed Milling Processes or a Positive Answer to Davies, Pratt, Dutterer and Burns," Journal of Manufacturing Science and Engineering, 126(3), pp. 481-487.
- [55] Insperger, T., and Stépán, G., 2004, "Updated semi-discretization method for periodic delay-differential equations with discrete delay," International Journal for Numerical Methods in Engineering, 61(1), pp. 117-141.
- [56] Zhao, M. X., and Balachandran, B., 2001, "Dynamics and stability of milling process," International Journal of Solids and Structures, 38(10), pp. 2233-2248.
- [57] Honeycutt, A., and Schmitz, T., 2016, "A Numerical and Experimental Investigation of Period-n Bifurcations in Milling," Journal of Manufacturing Science and Engineering, 139(1), pp. 011003-011003-011011.
- [58] Honeycutt, A., and Schmitz, T. L., 2016, "Experimental Validation of Period-n Bifurcations in Milling," Procedia Manufacturing, 5, pp. 362-374.
- [59] Honeycutt, A., and Schmitz, T., 2016, "A new metric for automated stability identification in time domain milling simulation," ASME Journal of Manufacturing Science and Engineering,, 138/7, p. 074501.
- [60] Honeycutt, A., and Schmitz, T. L., 2016, "Milling Stability Interrogation by Subharmonic Sampling," Journal of Manufacturing Science and Engineering, 139(4), pp. 041009-041009-041009.
- [61] Honeycutt, A., and Schmitz, T. L., 2017, "A Study of Milling Surface Quality during Period-2 Bifurcations," Procedia Manufacturing, 10, pp. 183-193.
- [62] Roukema, J. C., and Altintas, Y., 2007, "Generalized modeling of drilling vibrations. Part I: Time domain model of drilling kinematics, dynamics and hole formation," International Journal of Machine Tools & Manufacture, 47(9), pp. 1455-1473.
- [63] Altintas, Y., and Ko, J. H. J. C. A.-M. T., 2006, "Chatter stability of plunge milling," 55(1), pp. 361-364.
- [64] Altintas, Y., 2001, "Analytical Prediction of Three Dimensional Chatter Stability in Milling," JSME International Journal Series C Mechanical Systems, Machine Elements and Manufacturing, 44(3), pp. 717-723.

- [65] Altintas, Y., Shamoto, E., Lee, P., and Budak, E., 1999, "Analytical prediction of stability lobes in ball end milling," *Journal of Manufacturing Science and Engineering-Transactions of the Asme*, 121(4), pp. 586-592.
- [66] Jensen, S. A., and Shin, Y. C., 1999, "Stability Analysis in Face Milling Operations, Part 1: Theory of Stability Lobe Prediction," *Journal of Manufacturing Science and Engineering*, 121(4), pp. 600-605.
- [67] Ozturk, E., Budak, E., and Engineering, 2010, "Dynamics and stability of five-axis ball-end milling," *Trans ASME Journal of Manufacturing Science and Engineering*, 132/2, p. 021003.
- [68] Chao, S., and Altintas, Y., 2016, "Chatter free tool orientations in 5-axis ball-end milling," *International Journal of Machine Tools & Manufacture*, 106, pp. 89-97.
- [69] Sims, N. D., 2007, "Vibration absorbers for chatter suppression: A new analytical tuning methodology," *Journal of Sound and Vibration*, 301(3-5), pp. 592-607.
- [70] Yang, Y., Munoa, J., and Altintas, Y., 2010, "Optimization of multiple tuned mass dampers to suppress machine tool chatter," *International Journal of Machine Tools & Manufacture*, 50(9), pp. 834-842.
- [71] Slavicek, J., 1965, "The effect of irregular tooth pitch on stability in milling," *6th Machine Tool Design and Research Conference*, pp.15-22.
- [72] Opitz, H., "Improvement of the dynamic stability of the milling process by irregular tooth pitch," *Proc. Proc. 7th Int. MTDR Conference* pp. 213-227.
- [73] Vanherck, P., "Increasing Milling Machine Productivity by Use of Cutters with Non Constant Cutting Edge Pitch," *Proc. Proceedings of the 8th MTDR Conference*, pp. 947-960.
- [74] Tlusty, J., Ismail, F., and Zaton, W., "Use of special milling cutters against chatter," *Proc. NAMRC*, pp. 408-415.
- [75] Altintas, Y., Engin, S., and Budak, E., 1999, "Analytical stability prediction and design of variable pitch cutters," *Journal of Manufacturing Science and Engineering-Transactions of the Asme*, 121(2), pp. 173-178.
- [76] Olgac, N., and Sipahi, R., 2007, "Dynamics and Stability of Variable-pitch Milling," *Journal of Vibration and Control*, 13(7), pp. 1031-1043.
- [77] Budak, E., 2003, "An Analytical Design Method for Milling Cutters With Nonconstant Pitch to Increase Stability, Part I: Theory," *Journal of Manufacturing Science and Engineering*, 125(1), pp. 29-34.
- [78] Iglesias, A., Dombovari, Z., Gonzalez, G., Munoa, J., and Stepan, G., 2019, "Optimum selection of variable pitch for chatter suppression in face milling operations," *Materials*, 12(1), p. 112.
- [79] Comak, A., and Budak, E., 2017, "Modeling dynamics and stability of variable pitch and helix milling tools for development of a design method to maximize chatter stability," *Precision Engineering*, 47, pp. 459-468.
- [80] Sims, N. D., Mann, B., and Huyanan, S., 2008, "Analytical prediction of chatter stability for variable pitch and variable helix milling tools," *Journal of Sound and Vibration*, 317(3), pp. 664-686.
- [81] Turner, S., Merdol, D., Altintas, Y., and Ridgway, K., 2007, "Modelling of the stability of variable helix end mills," *International Journal of Machine Tools and Manufacture*, 47(9), pp. 1410-1416.
- [82] Dombovari, Z., and Stépán, G., 2012, "The Effect of Helix Angle Variation on Milling Stability," *Trans. ASME Journal of Manufacturing Science and Engineering*, 134/5, p. 051015.

- [83] Merdol, S. D., and Altintas, Y., 2004, "Mechanics and dynamics of serrated cylindrical and tapered end mills," *Journal of Manufacturing Science and Engineering-Transactions of the Asme*, 126(2), pp. 317-326.
- [84] Dombovari, Z., Altintas, Y., and Stepan, G., 2010, "The effect of serration on mechanics and stability of milling cutters," *International Journal of Machine Tools & Manufacture*, 50(6), pp. 511-520.
- [85] Tehranizadeh, F., Koca, R., and Budak, E., 2019, "Investigating effects of serration geometry on milling forces and chatter stability for their optimal selection," *International Journal of Machine Tools Manufacture*, p. 103425.
- [86] Lazoglu, I., Vogler, M., Kapoor, S. G., and DeVor, R. E., 1998, "Dynamics of the simultaneous turning process," *Trans. Am. Res. Inst. SME*, pp. 135-140.
- [87] Budak, E., and Ozturk, E., 2011, "Dynamics and stability of parallel turning operations," *CIRP Annals*, 60(1), pp. 383-386.
- [88] Ozturk, E., Comak, A., and Budak, E., 2016, "Tuning of tool dynamics for increased stability of parallel (simultaneous) turning processes," *Journal of Sound and Vibration*, 360, pp. 17-30.
- [89] Reith, M. J., Bachrathy, D., and Stepan, G., 2016, "Optimal Detuning of a Parallel Turning System—Theory and Experiments," *Trans ASME Journal of Dynamic Systems, Measurement, and Control*, 139/1(1), pp. 014503-014503-014507.
- [90] Brecher, C., Epple, A., Neus, S., and Fey, M., 2015, "Optimal process parameters for parallel turning operations on shared cutting surfaces," *International Journal of Machine Tools and Manufacture*, 95, pp. 13-19.
- [91] Azvar, M., and Budak, E., 2017, "Multi-dimensional chatter stability for enhanced productivity in different parallel turning strategies," *International Journal of Machine Tools and Manufacture*, 123, pp. 116-128.
- [92] Shamoto, E., Mori, T., Sencer, B., Suzuki, N., and Hino, R., 2013, "Suppression of regenerative chatter vibration in multiple milling utilizing speed difference method—Analysis of double-sided milling and its generalization to multiple milling operations," *Precision Engineering*, 37/3, pp. 580-589.
- [93] Budak, E., Comak, A., and Ozturk, E., 2013, "Stability and high performance machining conditions in simultaneous milling," *CIRP Annals*, 62/1, pp. 403-406.
- [94] Yun, I. S., Wilson, W. R. D., and Ehmann, K. F., 1998, "Review of chatter studies in cold rolling," *International Journal of Machine Tools & Manufacture*, 38(12), pp. 1499-1530.
- [95] Thaler, T., Krese, B., and Govekar, E., 2015, "Stability diagrams and chatter avoidance in horizontal band sawing," *Cirp Annals-Manufacturing Technology*, 64(1), pp. 81-84.
- [96] Schmitz, T., and Donaldson, R., 2000, "Predicting High-Speed Machining Dynamics by Substructure Analysis," *Annals of the CIRP*, 49/1, pp. 303-308.
- [97] Schmitz, T., and Duncan, G. S., 2005, "Three-Component Receptance Coupling Substructure Analysis for Tool Point Dynamics Prediction, , " *Trans. ASME , Journal of Manufacturing Science and Engineering*, 127/4, pp. 781-790.
- [98] Cheng, C.-H., Duncan, G.S., and Schmitz, T., , 2007, "Rotating Tool Point Frequency Response Prediction using RCSA," *Machining Science and Technology*, 11(3), pp. 433-446.
- [99] Ozsahin, O., and Altintas, Y., 2015, "Prediction of frequency response function (FRF) of asymmetric tools from the analytical coupling of spindle and beam models of holder and tool," *International Journal of Machine Tools & Manufacture*, 92, pp. 31-40.

- [100] Comak, A., Ozsahin, O., and Altintas, Y., 2016, "Stability of Milling Operations With Asymmetric Cutter Dynamics in Rotating Coordinates," *Journal of Manufacturing Science and Engineering-Transactions of the Asme*, 138(8).
- [101] Namazi, M., Altintas, Y., Abe, T., and Rajapakse, N., 2007, "Modeling and identification of tool holder-spindle interface dynamics," *International Journal of Machine Tools & Manufacture*, 47(9), pp. 1333-1341.
- [102] Postel, M., Özsahin, O., and Altintas, Y., 2018, "High speed tooltip FRF predictions of arbitrary tool-holder combinations based on operational spindle identification," *International Journal of Machine Tools & Manufacture*, 129, pp. 48-60.
- [103] Ozsahin, O., Budak, E., and Ozguven, H. N., 2015, "In-process tool point FRF identification under operational conditions using inverse stability solution," *International Journal of Machine Tools and Manufacture*, 89, pp. 64-73.
- [104] Law, M., Phani, A. S., and Altintas, Y., 2013, "Position-Dependent Multibody Dynamic Modeling of Machine Tools Based on Improved Reduced Order Models," *Trans. ASME Journal of Manufacturing Science and Engineering*, 135/2, p. 021008.
- [105] Cordes, M., Hintze, W., and Altintas, Y., 2019, "Chatter stability in robotic milling," *Robotics and Computer-Integrated Manufacturing*, 55, pp. 11-18.
- [106] Law, M., Ihlenfeldt, S., Wabner, M., Altintas, Y., and Neugebauer, R., 2013, "Position-dependent dynamics and stability of serial-parallel kinematic machines," *CIRP Annals-Manufacturing Technology*, 62/1, pp. 375-378.
- [107] Tuysuz, O., and Altintas, Y., 2018, "Time-Domain Modeling of Varying Dynamic Characteristics in Thin-Wall Machining Using Perturbation and Reduced-Order Substructuring Methods," *Trans. ASME Journal of Manufacturing Science*, 140(1), p. 011015.
- [108] Moriwaki, T., 2008, "Multi-functional machine tool," *CIRP Annals*, 57/2, pp. 736-749.
- [109] Comak, A., and Altintas, Y., 2018, "Dynamics and Stability of Turn-Milling Operations With Varying Time Delay in Discrete Time Domain," *Transactions of the ASME, Journal of Manufacturing Science and Engineering*, 140/10.
- [110] Iglesias, A., Munoa, J., and Ciurana, J., 2014, "Optimisation of face milling operations with structural chatter using a stability model based process planning methodology," *The International Journal of Advanced Manufacturing Technology*, 70(1-4), pp. 559-571.
- [111] Jin, X., and Altintas, Y., 2013, "Chatter Stability Model of Micro-Milling With Process Damping," *Journal of Manufacturing Science and Engineering-Transactions of the Asme*, 135(3).
- [112] Ahmadi, K., and Altintas, Y., 2013, "Stability of lateral, torsional and axial vibrations in drilling," *International Journal of Machine Tools & Manufacture*, 68, pp. 63-74.
- [113] Wan, M., Kilic, Z. M., and Altintas, Y., 2015, "Mechanics and Dynamics of Multifunctional Tools," *Journal of Manufacturing Science and Engineering-Transactions of the Asme*, 137(1).
- [114] Kilic, Z. M., and Altintas, Y., 2016, "Generalized mechanics and dynamics of metal cutting operations for unified simulations," *International Journal of Machine Tools & Manufacture*, 104, pp. 1-13.
- [115] Khoshdarregi, M. R., and Altintas, Y., 2018, "Dynamics of Multipoint Thread Turning-Part I: General Formulation," *Journal of Manufacturing Science and Engineering-Transactions of the Asme*, 140(6).

[116] Katz, A., Erkorkmaz, K., Ismail, F. J. J. o. M. S., and Engineering, 2018, "Virtual Model of Gear Shaping—Part I: Kinematics, Cutter–Workpiece Engagement, and Cutting Forces," 140(7), p. 071007.

[117] No, T., Gomez, M., Copenhaver, R., Uribe Perez, J., Tyler, C., and Schmitz, T., 2019, "Force and Stability Modeling for Non-standard Edge Geometry Endmills," ASME Journal of Manufacturing Science, 141(12), p. 121002.

FIGURE CAPTIONS

Figure 1 Dynamics of orthogonal cutting system. a) Regenerative mechanism. b) Process damping mechanism

Figure 2 Block diagram of dynamic orthogonal cutting with process damping and regenerative chip feedback.

Figure 3 Chatter stability diagrams and corresponding chatter frequency diagram for mode coupling chatter, and regenerative chatter with and without process damping. Simulation parameters: Cutting coefficients - $K_t=1000$ MPa, $K_r=0.3$; Modal parameters- $k_1=15\times 10^6$ N/m, $k_2=10\times 10^6$ N/m, . The orientation of flexibilities- , ; process damping constant - $C_p=2e6$ N/m; workpiece diameter = 30 mm. Simulated cases: Cases- A: $n=700$ rev/min (stable, process damping zone), B: $n=5000$ rev/min (stable, high speed zone), C: $n=8000$ rev/min (unstable, high speed zone).

Figure 4. Theoretical stability chart of turning processes in the plane of the dimensionless spindle speed and the dimensionless depth of cut . The dimensionless chatter frequency is greater than 1. The damping ratio is fixed at , while refers to the sequence number of the lobes.

Figure 5 Dynamic model of highly interrupted cutting

Figure 6 Theoretical stability chart of highly interrupted cutting in the plane of the dimensionless spindle speed and the dimensionless (axial) depth of cut . The dimensionless chatter frequencies are . The damping ratio is fixed at , .

Figure 7 Dynamics of milling

Figure 8 Stability lobes predicted with the zero-order solution analytically and time-domain numerical simulations for a cutter with two circular inserts.

Figure 9 Comparison of zero-order and multi-frequency with three harmonics stability lobe solutions. The cutter has three teeth with a diameter of 23.6 mm used in down milling of Al6061 material ($=500$ MPa, $=0.3$) with a feed rate of 0.120 mm/rev/tooth and a radial depth of 1.256 mm. The structure is assumed to be flexible in y (normal) direction only with $=1.4\times 10^6$ N/m, $=907$ Hz, $=0.017$.

Figure 10 Discretization of the time-periodic function $A(t)$ by piece-wise constant step-function (a), and the discretization of the constant time delay T by time-periodic delay (b).

Figure 11 Stability chart of the milling process. The period-doubling lobes become unstable islands. Feed per tooth is 0.1 mm, radial immersion is 0.02, a number of cutting edges is , the cutting coefficients are MPa and , the damping ratio is .

Figure 12 Top) Time-domain results for a period-2 bifurcation, i.e. chatter with added lobes. (Bottom) Poincaré map for period-2 bifurcation. The sampled points align at a two fixed locations for the period-2 bifurcation.

Figure 13 Example bifurcation diagram. Stable behavior is observed up to an axial depth (b) of approximately 2.5 mm. It is indicated by the single value of the sampled feed direction (x) tool displacements. Between 2.5 mm and 4 mm, secondary Hopf chatter with added lobes occurs (i.e., a distribution of sampled points). Between 4 mm and 5.5 mm, a period-3 bifurcation is seen (i.e., three distinct sampled points).

Figure 14 Dynamic flexibilities of a twist drill and milling cutter with circular inserts.

Figure 15 Rectilinear representation of variable pitch milling tool proposed by Slavicek [71].

Figure 16 Effect of $\square \square$ on stability gain for a four-tooth end mill with linear pitch variation.

Figure 17. The effect of pitch angle variation on the stable depth of cut for different spindle speeds and on the chatter frequency [77].

Figure 18 Chatter stability of regular and serrated end mills, after Merdol et al. [81].

Figure 19 (a) Parallel turning [85] and (b) parallel milling operations [92].

Figure 20 (a) parallel turning configuration, (b) stability lobe diagram for a1 versus spindle speed (n) when a2= 1.5 mm and (c) time-domain simulation for different points f (unstable), e (stable) and d (unstable).(From [85])

Figure 21 Predicted stability lobe diagram and the experimental results